T.C.

ÇANAKKALE ONSEKİZ MART UNIVERSITY

SCHOOL OF GRADUATE STUDIES

DEPARTMENT OF MOLECULAR BIOLOGY AND GENETICS

INVESTIGATING THE THERAPEUTIC ACTIVITIES OF NOVEL SELAGIBENZOPHENONE B DERIVATIVES AS PARP-1 INHIBITORS IN THE TREATMENT OF CASTRATION-RESISTANT PROSTATE CANCER

MASTER OF SCIENCE

HAZAL NAZLICAN ATALAY

Thesis Supervisor

PROF.DR. TUĞBA TÜMER

Co-Supervisor

ASSOC.PROF. MEHMET ÖZBİL

ÇANAKKALE – 2024

T.C.
ÇANAKKALE ONSEKİZ MART UNIVERSITY
SCHOOL OF GRADUATE STUDIES

DEPARTMENT OF MOLECULAR BIOLOGY AND GENETICS

INVESTIGATING THE THERAPEUTIC ACTIVITIES OF NOVEL SELAGIBENZOPHENONE B DERIVATIVES AS PARP-1 INHIBITORS IN THE TREATMENT OF CASTRATION-RESISTANT PROSTATE CANCER

MASTER OF SCIENCE THESIS

HAZAL NAZLICAN ATALAY

Thesis Supervisor
PROF.DR. TUĞBA TÜMER
Co-Supervisor
ASSOC.PROF. MEHMET ÖZBİL

This study has been supported by the Scientific Research Project Coordination Unit of Turkey 2210/C National MSc Scholarship Program, Çanakkale Onsekiz Mart University Scientific Research Project Coordination Unit (Project No: YL-2023-4406) and Türkiye Health Institues (Project No: TUSEB-B-22842).

ÇANAKKALE – 2024

T.C.
ÇANAKKALE ONSEKİZ MART ÜNİVERSİTESİ
LİSANSÜSTÜ EĞİTİM ENSTİTÜSÜ

Hazal Nazlıcan ATALAY tarafından Prof. Dr. Tuğba BOYUNEĞMEZ TÜMER yönetiminde ve Doç. Dr. Mehmet ÖZBİL ikincil danışmalığında hazırlanan ve **09/08/2024** tarihinde aşağıdaki jüri karşısında sunulan "**Investigating The Therapeutic Activities Of Novel Selagibenzophenone B Derivatives As Parp-1 Inhibitors In The Treatment Of Castration-Resistant Prostate Cancer**" başlıklı çalışma, Çanakkale Onsekiz Mart Üniversitesi Lisansüstü Eğitim Enstitüsü **Moleküler Biyoloji ve Genetik Anabilim Dalı**'nda **YÜKSEK LİSANS** olarak oy birliği ile kabul edilmiştir.

Jüri Üyeleri	**İmza**
Prof. Dr. Tuğba BOYUNEĞMEZ TÜMER (Danışman)	
Prof. Dr. Kemal Melih TAŞKIN	
Prof. Dr. Şevki ARSLAN	

Tez No : 10613309
Tez Savunma Tarihi : 09/08/2024

Prof. Dr. Ahmet Evren ERGİNAL
Enstitü Müdürü

../../20..

ETİK BEYAN

Çanakkale Onsekiz Mart Üniversitesi Lisansüstü Eğitim Enstitüsü Tez Yazım Kuralları'na uygun olarak hazırladığım bu tez çalışmasında; tez içinde sunduğum verileri, bilgileri ve dokümanları akademik ve etik kurallar çerçevesinde elde ettiğimi, tüm bilgi, belge, değerlendirme ve sonuçları bilimsel etik ve ahlak kurallarına uygun olarak sunduğumu, tez çalışmasında yararlandığım eserlerin tümüne uygun atıfta bulunarak kaynak gösterdiğimi, kullanılan verilerde herhangi bir değişiklik yapmadığımı, bu tezde sunduğum çalışmanın özgün olduğunu, bildirir, aksi bir durumda aleyhime doğabilecek tüm hak kayıplarını kabullendiğimi taahhüt ve beyan ederim.

PLAGIARISM DECLARATION

I hereby affirm that all the information and results presented in the visual and written forms have been obtained by myself in accordance with the established academic and ethical standards. Furthermore, all other results and information referenced in the thesis that are not specific to this study have been duly cited.

Hazal Nazlıcan ATALAY

09/08/2024

ACKNOWLEGMENTS

First of all, I would like to thank my supervisor Prof. Dr. Tuğba Tümer, whom I have been working with for 3.5 years and will hopefully continue to work with. Thanks to her, I have worked on many projects and publications. I am grateful to her for always trying to bring out the best in us, even if we cannot see the light within ourselves at times. I would like to thank her for showing us that always having a dream and a story takes us much further with her motto, Thoughts become things.

I would also like to thank my second supervisor Assoc. Prof. Mehmet Özbil. I would like to thank him for guiding me on computer-based analyses, which I have wanted for a long time and which have always been a subject of curiosity and for always being supportive and patient instructive in areas where I was lacking.

I would like to thank Öznur Salatacı, my roommate for three years and my friend for eight years, for never withholding her support, patience and friendship.

I would like to thank Serhat, who started my undergraduate education and laboratory at the same time, for always being supportive and believing in me more than I did even when I didn't believe in myself.

I would like to thank Berkay and Özlem, who have taught me everything since the moment I started the laboratory, for always being good teachers and patiently allowing us to learn.

I would also like to thank Kübra, Raşit and Taylan, who are in our neighboring laboratory but whom I can always ask anything to and who support me without hesitation.

Even though Berkay, Serhat, Özlem, Kübra and Raşit are currently in different countries, knowing that our hearts are always together will always be hopeful for me.

I would also like to thank Assit.Prof. Seda Kulabaş, who has always been careful to listen to me and never withholds her help, even though we have just met, for her support.

I would also like to thank my labmates Orçun, Efe, Erol and Zeynep, who I am currently working with, for being patient during my thesis period and always supporting me.

As a special thank to Gizem, who is a PhD student of Assoc. Prof. Mehmet Özbil's, for teaching me so much and always being able to ask me anything.

I would like to thank all the former and new members of ÇOMÜ Theater Club, which I have been a part of for eight years, which have shown me that dreaming and making my dream come true is an invaluable blessing. I would also like to thank our Theater Club academic supervisor Assist. Prof. Halife Çağlar for never withholding his support and ideas from me and always supporting me to be better.

I would like to thank my mother Çiğdem Atalay and my father Hakan Atalay, who brought me into this world and always allowed me to make my own decisions, who trusted me and never withheld their support..

Finally, I wish to acknowledge the financial support given by COMU Scientific Research Projects Coordination Unit (Project No: FYL-2023-4406). I am also thankful to the National MSc Scholarship Program (Program code: 2210-C) granted by Scientific Research Project Coordination Unit of Turkey (TUBITAK) and TUBITAK ULAKBIM for allowing me to access High Performance and Grid Computing Center (TRUBA resources).

Hazal Nazlıcam ATALAY

Çanakkale/2024

ÖZET

ÖZGÜN SELAGİBENZOFENON B TÜREVLERİNİN PARP-1 İNHİBİTÖRÜ OLARAK TERAPÖTİK ETKİNLİKLERİNİN KASTRASYON DİRENÇLİ PROSTAT KANSERİ TEDAVİSİNDE ARAŞTIRILMASI

Hazal Nazlıcan ATALAY
Çanakkale Onsekiz Mart Üniversitesi
Lisansüstü Eğitim Enstitüsü
Moleküler Biyoloji ve Genetik Anabilim Dalı Yüksek Lisans Tezi

Danışman: Prof. Dr. Tuğba TÜMER
İkinci Danışman: Doç. Dr. Mehmet ÖZBİL
09/08/2024,63

Zengin bir tıbbi geçmişe sahip ve çok çeşitli bir cins olan *Selaginella,* kanser tedavisi de dahil olmak üzere geleneksel ilaçlarda kullanılmıştır. Önceki araştırmalarımıza dayanarak, Selagibenzofenon B (SB) analoglarının bazılarının prostat kanseri hücrelerini seçici olarak hedefleme potansiyelini belirledik. *In siliko* çalışmalar yoluyla, yeni SB türevleri tasarladık ve bunların PARP-1'i umut verici bir hedef olarak ortaya koyduğunu bulduk. Geleneksel tedavilere karşı dirençli olduğu bilinen bir kanser türü olan kastrasyona dirençli prostat kanseri (CRPC) durumunda, PARP-1'i inhibe etmeye odaklanan hedefli tedavilerde umut vardır. Amacımız, PARP-1'i etkili bir şekilde inhibe edebilen bileşikleri keşfetmektir. Öncü SB türevleri, sağlıklı hücreler üzerinde minimum etkiye sahipken, prostat kanseri hücre hatlarında hücre sağ kalımı, göçü ve koloni oluşumunu seçici olarak inhibe etti. Ek olarak, *in siliko* moleküler kenetlenme ve dinamik çalışmaları, öncü bileşik ile PARP-1 arasında yüksek bir bağlanma afinitesi olduğunu ortaya koydu. Özetle, SB'ler PARP-1 inhibitörleri olarak hizmet etme potansiyeline sahiptir ve aday kanser önleyici ajanlar olarak daha da geliştirilebilir.

Anahtar Kelimeler: Kastrasyon dirençli prostat kanseri, PARP-1, Selagibenzofeno

ABSTRACT

INVESTIGATING THE THERAPEUTIC ACTIVITIES OF NOVEL SELAGIBENZOPHENONE B DERIVATIVES AS PARP-1 INHIBITORS IN THE TREATMENT OF CASTRATION-RESISTANT PROSTATE CANCER

Hazal Nazlıcan ATALAY

Çanakkale Onsekiz Mart University
School of Graduate Studies
Master of Science Thesis in Molecular Biology and Genetics

Supervisor: Prof. Dr. Tuğba TÜMER

Co-supervisor: Assoc. Prof. Mehmet ÖZBİL

09/08/2024, 63

Selaginella, a diverse genus with a rich medicinal history, has been used in traditional remedies, including for cancer treatment. Based on our previous research, we have identified the potential of some of the Selagibenzophenone B (SB) analogs to selectively target prostate cancer cells. Through *in silico* studies, we have designed novel SB derivatives and found that they reveal PARP-1 as a promising target. In the case of castration-resistant prostate cancer (CRPC), a type of cancer that is notoriously resistant to conventional treatments , there is hope in targeted therapies that focus on inhibiting PARP-1. Our objective is to discover compounds that can effectively inhibit PARP-1. The lead SB derivatives exhibited selective inhibition of cell survival, migration, and colony formation in prostate cancer cell lines, while having minimal effect on healthy cells. In addition, *in silico* molecular docking and dynamics studies revealed a high binding affinity between the lead compound and PARP-1. In summary, SBs possess the potential to serve as PARP-1 inhibitors and can be further developed as candidate anticancer agents.

Keywords: Castration-resistant prostate cancer, PARP-1, Selagibenzophenone

TABLE OF CONTENTS

Page No

THESIS DEFENCE EXAM RESULT FORM..……..... i
PLAGIARISM DECLARATION……..... ii
ACKNOWLEGMENTS……..... iii
ÖZET ……..…….... iv
ABSTRACT …… v
TABLE OF CONTENT..…….....…..……. vi
ABBREVIATIONS.....…….....…….…….... viii
LIST OF TABLES...……..... ix
LIST OF FIGURES……..……...……....…….. x

CHAPTER 1
INTRODUCTION 1

1.1. Molecular Etiology of Prostate Cancer..... 1
1.1.1. Inherited and Somatic Mutations……..... 2
1.1.2. Epigenetic Changes..... 3
1.1.3. Other Genetic Changes..... 4
1.1.4. Androgen Receptor (AR) Signaling..... 6
1.2. Castration-Resistant Prostate Cancer (CRPC) 7
1.2.1. Treatments of CRPC..... 8
1.2.2. PARP-1 Inhibitors (PARPi)..... 9
1.3. *In silico* Molecular Dynamics and Docking Simulations..... 13
1.4. Aim Of The Thesis..... 16

CHAPTER 2
PREVIOUS STUDIES 18

CHAPTER 3
MATERIALS AND METHODS 20

3.1. Materials..... 20
3.1.1. Chemicals and Kits..... 20
3.1.2. Equipments..... 20
3.2 Methods..... 21
3.2.1. Cell Culture Conditions..... 21
3.2.2. Cell Cytotoxicity Analyses..... 22
3.2.3. Colony Formation Assay..... 23
3.2.4. Wound Healing Assay..... 23
3.2.5. Gene Expression Analysis..... 24
3.2.6. PARP- 1 Inhibition Assay 24
3.2.7. *In silico* Studies 25
Molecular Dynamics (MD) Simulations..... 25
Molecular Docking Simulations..... 26
3.2.8. Statistical Analyses 26

CHAPTER 4
RESULTS AND DISCUSSION 27

4.1. Results of Biological Experiments..... 27
4.1.1. Determination of the Cytotoxic Effects of Novel SB Derivatives..... 27
4.1.2. Effect of Lead Compounds on Colony Formation Capacity..... 29
4.1.3. Effect of Lead Compounds on Wound Healing Capacity..... 31
4.1.4. Effects of SB Derivatives on Relative mRNA Expression Levels of Apoptotic Genes..... 35
4.1.4. Effects of SB Derivatives on Relative mRNA Expression Levels of Autophagic Genes..... 39
4.1.5. PARP-1 Inhibition Capacities of The Selective SB Derivatives..... 41
4.2. Results of *In silico* Studies..... 44
4.2.1. MD Simulations of PARP-1 Protein..... 44
4.2.2. Molecular Docking Studies..... 46

4.2.3. MD Simulations After Molecular Docking Studies..... 48
4.2.4. Root-Mean Square Fluctuation Analysis..... 50
4.3. Discussion..... 51

CHAPTER 5
CONCLUSION 56

REFERENCES……..... 57
BIOGRAPHY…….. I

ABBREVIATIONS

°C	Degree Celsius
ADT	Androgen Deprivation Therapy
ANOVA	One-way Analysis of Variance
AR	Androgen Receptor
ARE	Androgen-responsive Elements
cAMP	Cyclic Adenosine Monophosphate
cDNA	Complementary DNA
CRPC	Castration-Resistant Prostate Cancer
CVB3	Coxsackie Virus B3
GSTP1	Glutathione S-Transferase P1
H3K27me3	Trimethylation Of Lysine 27 Of Histone H3
HIF	Hypoxia-Inducible Factor
HOXB13	Homeobox13
IC_{50}	Half Maximal Inhibitory Concentration
LBD	Ligand Binding Domain
LGA	Lamarckian Genetic Algorithm
lncRNAs	Long Non-Coding RNAs
MD	Molecular Dynamics
miRNAs	Micrornas
mTOR	Mammalian Target Of Rapamycin
MYC	Myelocytoma
ncRNAs	Non-Coding Rnas
NKX3.1	Nk3 Homeobox 1
PARP-1	Poly [ADP-Ribose] Polymerase 1
PSMA	Prostate-Spesific Membrane Antigen
PTEN	Phosphate And Tensin Homolog
qPCR	Quantitative Polymerase Chain Reaction
RB1	Retinoblastoma 1
RMSD	Root-Mean-Square Deviation
RMSF	Root-Mean-Square Fluctuation
RTK	Receptor Tyrosine Kinases

SRB	Sulforhodamine B
TCA	Trichloroaceticacid
TP53	Tumor Protein P53
U	Units Of Enzyme
µg	Microgram
µl	Microliter

LIST OF TABLES

Table No	Table Name	Page No
Table 1	Chemicals and kits with catalogue numbers	20
Table 2	Equipment and devices with brand and model numbers	21
Table 3	IC_{50} values and selectivity indexes of SB derivatives	29
Table 4	PARP-1 IC_{50} values of the selective SB derivatives	43
Table 5	Binding affinities of the protein-ligands after molecular docking simulations	47
Table 6	Binding energies of the 3-AB and SB-7 compounds after protein-ligand MD simulations.	49

LIST OF FIGURES

Figure No	Figure Name	Page No
Figure 1	PARP-1's role in single-stranded DNA repair mechanism	10
Figure 2	Flowchart of the target prediction	13
Figure 3	Flowchart of the study	17
Figure 4	Structures of novel SB derivatives	22
Figure 5	Colony formation capacity of selective SB derivatives on DU145 cells	30
Figure 6	Colony formation capacity of selective SB derivatives on PC-3 cells	31
Figure 7	The effects of wound recovery capacities of the selective compounds on DU145 cells (A) SB-5, (B) SB-7, (C) SB-9, and (D) SB-10	33
Figure 8	The effects of wound recovery capacities of the selective compounds on PC3 cells (A) SB-5, (B) SB-7, (C) SB-9, and (D) SB-10	35
Figure 9	Relative mRNA expression levels of apoptotic genes on DU145 cells	37
Figure 10	Relative mRNA expression levels of apoptotic genes on DU145 cells	38
Figure 11	Relative mRNA expression levels of autophagic genes on DU145 cells	40
Figure 12	Relative mRNA expression levels of autophagic genes on PC-3 cells	41
Figure 13	PARP-1 inhibition capacities of the selective SB derivatives at 1-10-100 μM doses	42
Figure 14	PARP-1 inihibiton capacities of the SB-5, SB-7 and SB-10 compounds at 1-2000 μM doses	43
Figure 15	RMSD values of the PARP-1 protein structure at 200 ns time intervals	45

Figure 16	Cluster PARP-1 structure at 150-200 ns time intervals	46
Figure 17	2-D and 3-D structures of (A) 3- AB, and (B) SB-7 ligands	47
Figure 18	Representations of interactions between PARP-1, and (A) 3-AB, (B) SB-7	48
Figure 19	RMSD values of the 3-AB (A), and SB-7 (B) protein-ligands	48
Figure 20	Representations of interactions between PARP-1, and (A) 3-AB, (B) SB-7 after MD simulations	49
Figure 21	RMSF analysis of PARP-1 and 3-AB (protein-ligand structure) after MD simulations	50
Figure 22	RMSF analysis of PARP-1 and SB-7 (protein-ligand structure) after MD simulations	50

CHAPTER 1
INTRODUCTION

Cancer is a significant global issue and is one of the primary causes of mortality. The 2023 Cancer Statistics report states that there were about 1,958,310 new instances of cancer diagnosed in the US, accounting for 609,820 cancer-related deaths. Particularly, prostate cancer ranks as the fourth most diagnosed cancer according to the World Cancer Research Fund. Looking ahead to 2024, estimates suggest that around 299,010 individuals will receive a diagnosis of prostate cancer, with an unfortunate prediction of 35,250 deaths due to this disease. Prostate cancer emerges as one of the most common types of cancer in men. It notably ranks as the second most prevalent cancer type in men, following lung cancer, and represents a significant cause of cancer-related fatalities.

Prostate cancer is a disease characterized by the uncontrolled growth of cells in the prostate gland. The prostate gland is a part of the male reproductive system which located in behind the bladder. Prostate cancer grows slowly, but some sorts can be aggressive and spread ahead the body. There are several forms of prostate cancer such as adenocarcinoma, small cell carcinoma and neuroendocrine tumors, hence adenocarcinoma is the most frequent one. Also, prostate cancer classified into four distinct stages which determine progression of the cancer. In Stage 1, the cancer is restricted to the prostate and normally has no symptoms. While in stage 2, the cancer remains in the prostate but may be bigger and more aggressive. Stage 3 cancer grows beyond the prostate and may metastase other tissues. In Stage 4, the cancer spreads to lymph nodes, bones, or organs. Prostate cancer has a complex molecular etiology involving genetic and epigenetic factors and dysregulated signaling pathways largely caused by a combination of inherited susceptibility, hormonal effects, and environmental factors.

1.1. Molecular Etiology of Prostate Cancer

Prostate cancer's molecular etiology consists of too many parameters such as inherited and somatic mutations, epigenetics changes, other genetic changes and androgen receptor signalling.

1.1.1. Inherited and Somatic Mutations

Mutations are significant factors in cancer development, with two general forms: inherited mutations and somatic mutations.

Inherited mutations thus are genetic changes that can be inherited from generation to generation and thereby cause a heightened vulnerability to suffering from prostate cancer. These mutations act as a stage of setting the prostate cancer. Key examples of inherited mutations are said to include mutations in the genes Breast cancer gene 1 (BRCA1), Breast cancer gene 2 (BRCA2), Homeobox13 (HOXB13), and Ataxia Telangiectasia Mutated (ATM). A number of other genes are attached to the DNA of both BRCA1 and BRCA2. In the exact determination of these sequences, homologous recombination is important. Most of these gene mutations might cause potential induction in DNA damage and genomic instability, while other studies report that mutations on BRCA2 increase the probability of prostate cancer (Kote-Jarai et al., 2011). The other mutation is HOXB13. The HOXB13 gene encodes a transcription factor that regulates prostate hormones. According to the study, this mutation raises the risk of prostate cancer by almost 20 times (Zuhlke et al., 2012). The last common mutation is ATM mutation. The ATM genes play a significant role in regulating DNA and cellular functions. ATM mutations can cause DNA damage and cancer formation, and ATM forms increase the risk of advanced prostate cancer, especially (Leongamornlert et al., 2012).

Somatic mutations are genetic changes acquired throughout life that cause cells to proliferate uncontrollably. A few of the somatic mutations frequently seen in prostate cancer are Tumor protein p53 (TP53), Phosphate and Tensin Homolog (PTEN), Retinoblastoma 1 (RB1) and TMPRSS2-ERG mutations. The TP53 gene plays a critical role in cell proliferation and apoptosis. These mutations lead to increased apoptosis. Researchers found that TP53 mutations can cause prostate cancer (Mello and Attardi, 2013). On the other hand, the PTEN gene has a negative correlation with the PI3K/AKT/mTOR pathway. PTEN and phosphatidylinositol (3,4,5)-triphosphate (PIP3) inhibit PI3K/AKT/mTOR signaling. According to Chen et al., PTEN mutations and activation can lead to a decrease in cell activity. Besides, the RB1 gene is responsible for several traits and controls the G1-S

pathway (Chen et al., 2018). According to Knudsen et al., RB1 mutations are associated with increased cell proliferation and control of cell division in prostate cancer (Knudsen et al., 2019) . TMPRSS2-ERG treatment improves prostate function by 50%. The study found that TMPRSS2 gene promoters play a pivotal role of the ERG gene transcription factor. According to Tomlins et al. , ERG expression leads to increased cell proliferation and invasion (Tomlins et al., 2005) .

1.1.2. Epigenetic Changes

Some epigenetic modifications influence the growth of prostate cancer. One of these processes is DNA methylation. DNA methylation occurs when a methyl group is added to the 5th carbon atom of the cytosine nucleotides of DNA, and this process inhibits gene expression. Excessive methylation in the promoter regions of tumor suppressor genes is common in prostate cancer, which contributes to their silence and cancer progression. One of the most prevalent epigenetic modifications seen in prostate cancer is methylation of the glutathione S-transferase P1 (GSTP1) promoter region. GSTP1 is an enzyme that protects cells from DNA damage. Methylation of this gene reduces GSTP1 expression and increases sensitivity to DNA damage (Brooks et al., 1998).

Additionally, modifications in histone proteins regulate chromatin structure and gene expression. These modifications include acetylation, methylation, phosphorylation, and ubiquitylation. Histone modifications in prostate cancer can cause significant changes in gene expression. For example, trimethylation of lysine 27 of histone H3 (H3K27me3) is a modification that promotes gene silencing and is catalyzed by the enzyme, enhancer of Zeste homolog 2 (E2H2). Overexpression of EZH2 in prostate cancer results in increased H3K27me3 levels and silencing of tumor suppressor genes (Varambally et al., 2002).

Furthermore, non-coding RNAs (ncRNAs) play a crucial role in the advancement of prostate cancer. These RNA molecules are essential for regulating gene expression post-transcriptionally. They are categorized into two main groups: microRNAs (miRNAs) and long non-coding RNAs (lncRNAs). MicroRNAs interact with target mRNAs, preventing

their degradation or translation. In prostate cancer, the expression levels of certain miRNAs may either increase or decrease. For instance, the upregulation of miR-21 has been shown to enhance cancer cell proliferation by downregulating tumor suppressor genes (Volinia et al., 2006). Additionally, long non-coding RNAs modulate gene expression through diverse mechanisms. In prostate cancer, specific lncRNAs like HOTAIR have been linked to metastasis and unfavorable prognosis (Gupta et al., 2010).

These epigenetic changes have a significant impact on the development, progression, and response to treatment of prostate cancer.

1.1.3. Other Genetic Changes

Other genetic alterations that play a role in prostate cancer development include the Myelocytoma (MYC), NK3 Homeobox 1 (NKX3.1), and Speckle-type pox virus and zinc finger (POZ) protein (SPOP). The MYC gene is an oncogene responsible for controlling cell growth, proliferation, and metabolism. Amplification of the MYC gene is common in prostate cancer and is associated with aggressive tumor characteristics (Schreiber et al., 2006). In the meantime, NKX3.1 is a prostate-specific tumor suppressor gene that maintains prostate development and differentiation. Its loss or mutation might be involved in increasing the susceptibility to prostate cancer (Kim et al., 2002). Additionally, SPOP is a nuclear genetic regulator that determines ubiquitin-mediated protein degradation. SPOP mutations are common in prostate cancer, which can cause increased cell proliferation by altering target protein degradations (Barbieri et al., 2012).

Prostate cancer development involves the disruption of various biochemical pathways and signaling networks, which in turn stimulate cell proliferation, survival, metastasis, and other related characteristics of cancer. One of these pathways is the PI3K/AKT/mTOR pathway, which plays a crucial role in controlling cellular growth, proliferation, survival, and metabolism.

When activated by cell surface receptors, PI3K converts phosphatidylinositol (4,5)-bisphosphate (PIP2) into phosphatidylinositol (3,4,5)-triphosphate (PIP3). PIP3, in turn, interacts with and activates protein kinase B (AKT). AKT phosphorylates several targets involved in cell growth, survival, and metabolism, including the mammalian target of rapamycin (mTOR). mTOR, a kinase existing in two forms (mTORC1 and mTORC2), governs cell proliferation and protein synthesis. While mTORC1 stimulates cell growth and protein synthesis, mTORC2 controls AKT activation and regulation of the cytoskeleton.

The activity of the PI3K/AKT/mTOR pathway is inhibited by PTEN, which dephosphorylates PIP3 back to PIP2. However, mutations or deletions in the PTEN gene can lead to excessive activation of this pathway, resulting in uncontrolled cell proliferation. It is common for prostate cancer to exhibit abnormal activation of the PI3K/AKT/mTOR pathway, with PTEN loss being one of the most prevalent changes observed. This excessive pathway activation promotes both the proliferation and survival of prostate cancer cells (Vivanco and Sawyers, 2002).

An additional pathway relevant to prostate cancer is the Wnt/β-Catenin pathway, which becomes active when Wnt proteins bind to Frizzled (Fzd) receptors on the cell surface. This binding triggers the activation of the Dishevelled (Dvl) protein and the suppression of the β-catenin destruction complex. Inhibiting this destruction complex leads to the accumulation of β-catenin in the cytoplasm before it enters the nucleus. Inside the nucleus, β-catenin interacts with TCF/LEF transcription factors, resulting in the activation of genes responsible for controlling cell proliferation and differentiation. In prostate cancer, the activation of the Wnt/β-catenin pathway encourages cell proliferation and the spread of cancer, with mutations or increased expression of components within this pathway contributing to the advancement of cancer growth.

Another pathway involved in prostate cancer is the RAS/RAF/MEK/ERK pathway. This pathway is initiated by the activation of RAS, a small GTPase that becomes active when it binds to GTP upon the activation of receptor tyrosine kinases (RTK) on the cell surface. Active RAS then stimulates RAF kinase, leading to its phosphorylation and activation. The

activated RAF kinase, in turn, phosphorylates and activates the MEK kinase. MEK kinase phosphorylates and activates the ERK kinase, which subsequently translocates into the nucleus. Inside the nucleus, ERK kinase phosphorylates and activates numerous transcription factors that control cell growth, proliferation, and differentiation.

In prostate cancer, the RAS/RAF/MEK/ERK pathway can become overactivated, promoting the proliferation and metastasis of cancer cells. Mutations in the RAS or RAF genes can perpetually activate this pathway, driving the growth of cancer cells (Mendoza et al., 2011).

Other pathways also contribute to prostate cancer progression. One of them is the Hypoxia-Inducible Factor (HIF) pathway which stabilizes HIF-1α in hypoxic conditions, allowing it to interact with HIF-1β to form a transcription factor complex that promotes the expression of genes involved in angiogenesis and metabolic adaptability. Researchers found that HIF-1α enhances tumor development and metastasis in prostate cancer patients (Rankin and Giaccia, 2016). The other pathway is Notch pathway that controls cell fate, proliferation, and differentiation. When Notch receptors bind to their ligands (Delta and Jagged), the intracellular domain (NICD) is released and transported to the nucleus, where it regulates the transcription of target genes. Dysregulation of the Notch pathway in prostate cancer may lead to increased cell proliferation and metastasis.

1.1.4. Androgen Receptor (AR) Signaling

The androgen receptor (AR) signalling pathway represents another crucial pathway implicated in the progression of prostate cancer. The role of AR signalling in the formation and advancement of prostate cancer is of critical importance. The binding of androgens, which are male sex hormones, to ARs affects the regulation of target genes. The AR protein acts as a transcription factor and is composed of multiple domains, including the Ligand Binding Domain (LBD), DNA Binding Domain (DBD), and N-terminal Activator Domain (NTD). Collectively, these domains stimulate the transcription of target genes.

The mechanism of AR signalling occurs in distinct stages. Androgens enter the cell membrane and bind to ARs, which are located in the cytoplasm. This binding process induces a structural alteration in ARs, which then form dimers. These activated AR dimers then move into the nucleus, where they bind to androgen-responsive elements (AREs) within the DNA, thereby initiating the transcription of target genes. It is believed that prostate cancer progression is influenced by multiple pathways that impact AR signalling. In prostate cancer cases, the AR gene is frequently overexpressed or amplified, which results in AR signalling despite low androgen levels (Koivisto et al., 1997). Changes in the AR gene can impact ligand binding specificity, resulting in androgen-independent AR activation and playing a significant role in the development of resistance to anti-androgen treatments. Specific AR isoforms, such as AR-V7, which lack the ligand-binding domain, can drive androgen-independent AR activation, leading to the development of treatment-resistant disease (Lian et al., 2015). The transcriptional activity of AR is regulated by various coactivator and corepressor proteins. An increase in coactivators or a deficiency in corepressors enhances AR signaling in prostate cancer.

Androgen Deprivation Therapy (ADT) is a sort of treatment strategy for prostate cancer that reduces androgen levels or inhibits AR activation. ADT can be achieved through surgical castration. Although ADT works initially, the condition often progresses to Castration-resistant prostate cancer (CRPC) . CRPC refers to prostate cancer that continues to progress despite ADT treatment. The formation of CRPC is linked to reactivation of AR signaling and other escape mechanisms. Therefore, CRPC is currently one of the most aggressive and challenging forms of prostate cancer to treat due to its typically poor prognosis. Researchers are increasingly focused on understanding and developing new treatment strategies for CRPC because of the urgent need for more effective therapies.

1.2. Castration-Resistant Prostate Cancer (CRPC)

CRPC represents an advanced stage of the disease that continues to progress even in the presence of decreased testosterone levels. The development of CRPC involves multiple resistance mechanisms, including the activation of pathways that are independent of the AR, intratumorally production of androgens, amplification and mutation of the AR. Notably, the amplification and mutation of AR in CRPC contribute to increased sensitivity to low levels

of androgens, enabling AR activity even in environments where androgen levels are low (Le et al., 2023). These resistance mechanisms play a crucial role in the progression and persistence of CRPC. These mutations and amplifications allow cancer cells to proliferate and survive despite androgen deprivation therapy (ADT), which supports the progression of the disease. ADT can be adapted by prostate cancer cells and prevent the adverse effects of systemic androgens by producing local androgens in the tumor microenvironment. Local androgen synthesis increases resistance and accelerates cancer progression by promoting the growth and spread of cancer cells. CRPC can trigger both AR-related and AR-independent mechanisms to increase the proliferation and viability of cancer cells making treatment strategies challenging.

1.2.1. Treatments of CRPC

One approach to treating CRPC involves the use of androgen synthesis inhibitors. Drugs like Abiraterone limit androgen production, thereby suppressing AR signaling. Abiraterone is a drug that inhibits testosterone synthesis, hence preventing prostate cancer cells from proliferating. However, the drug causes negative effects such as reducing blood pressure and potassium levels (de Bono et al., 2020a).

Another approach uses AR antagonists, such as enzalutamide, which inhibit AR binding to DNA and the transcription of target genes. Enzalutamide is a synthetic drug utilized in the treatment of CRPC as an AR inhibitor. Its mechanism of action involves targeting the AR signaling pathways, where AR is typically activated by androgen binding and transported to the cell nucleus. Enzalutamide disrupts this process by impeding the passage of AR to the nucleus, thereby inhibiting its regulation of gene transcription. Through this action, Enzalutamide effectively suppresses the expression of genes crucial for the proliferation and viability of cancer cells (Scher et al., 2012). However, similar to other drugs, this drug is associated with notable side effects. Some of these include an elevated risk of hypertension and seizures.

Another treatment strategy for the disease is a plant-based chemotherapeutics, such as docetaxel, and cabazitaxel. Docetaxel, a plant-based chemotherapeutic agent that basic

from *Taxus Baccata*, is widely used in cancer treatment due to its ability to stabilize microtubules and promote apoptosis. When combined with prednisone, it can extend life for individuals with CRPC. However, it has significant and common side effects like neutropenia and peripheral neuropathy. A distinct drug is Cabazitaxel which is similar to docetaxel, derived from from *Taxus Baccata*. Cabazitaxel stabilizes microtubules and prevents their depolymerization. This disrupts the separation of chromosomes during cell division and leads to the arrest of the cell cycle in the mitotic phase. Thus, it causes cancer cells to undergo apoptosis. Cabazitaxel is used in patients who develop resistance to docetaxel, but it has serious side effects such as bone marrow suppression, anemia and neutropenia (de Bono et.al., 2010) .

Recently a new approach, poly-ADP-ribose polymerase 1 (PARP-1) inhibitors (PARPi) has emerged in the treatment of CRPC. Ongoing research and clinical trials are focused on optimizing the use of PARPi and exploring combination therapies to improve outcomes in CRPC. This new treatment strategy represents a significant improvement in the management of this aggressive form of prostate cancer.

1.2.2. PARP-1 Inhibitors (PARPi)

The PARP family is an enzyme involved in DNA repair, and its inhibition can lead to the accumulation of DNA damage in cancer cells, ultimately causing cell death. PARP family consist of 17 enzymes which names PARP-1,2 etc. One of the significant one is PARP-1. The PARP-1 enzyme provides covalent binding to target proteins and PAR. Since PARP-1 activity is commonly dysregulated in various types of cancer, it offers a promising opportunity for cancer therapy. PARP-1 is activated due to DNA damage. ADP-ribose molecules bind together to form PAR chains, which help repair single-strand breaks and attract additional repair proteins. Consequently, DNA repair enzymes provide clues in locating the damage site (Rose et al., 2020). PARP-1 binds branched poly (ADP-ribose) (PAR) chains that help repair DNA strands and helps recruit other proteins during the repair process shown in Figure 1. A). This creates a signal that is detected by enzymes that aid in

DNA repair. PARP-1 also affects the cancer cell cycle by controlling cellular division and cell death processes such as necrosis, apoptosis, and necroptosis.

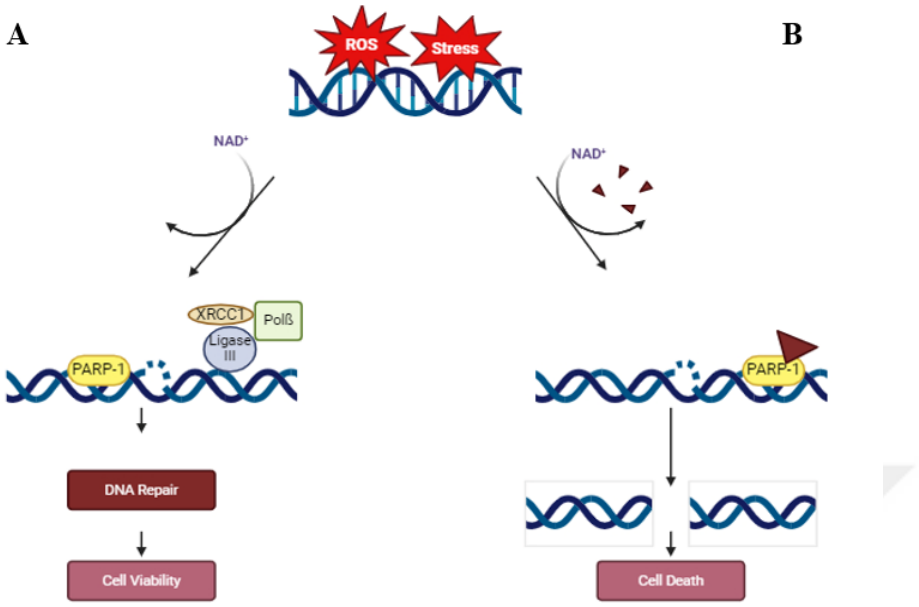


Figure 1. PARP-1's role in single-stranded DNA repair mechanism. A) normal function of PARP-1, B) PARP-1 inhibitors affect.

PARP-1 is significant due to its role in DNA repair mechanism. When the PAPRi's inhibited DNA repair mechanism, DNA wouldn't be able to repair single-strand breaks. As a results, it causes to apoptosis (shown in Figure 1- B). This sort of inhibition for PARP-1 can be a lead therapeutic approach to decrease cancer cell proliferation. PARP-1 can also affect AR signaling by inhibiting the activation of prostate-specific genes such as TMPRSS2-ERG and prostate-specific membrane antigen (PSMA), which are required for AR activation, especially in CRPC models. Considering its involvement in cancer cells, PARP-1 represents an important target, especially inhibition of PARP-1in the context of CRPC treatments.

In the market, there are several FDA approved PARP-1 inhibitors, such as olaparib, veriparib, rucaparib, and niraparib.

Suberoylanilide hydroxamic acid (SAHA), a histone deacetylase inhibitor, was administered alone or in combination with veliparib, another PARP-1 inhibitor, *in vivo and*

in vitro study involving prostate cancer and prostate epithelium cells. The findings revealed that veliparib plus SAHA treatment exceeded either medication alone. In an in vivo xenograft animal model created with DU145 cells, a type of CRPC cell line, combination medication therapy significantly slowed the growth of the malignancy (L. Yin et al., 2018). Furthermore, normal prostate epithelial cells showed no detectable toxicity when both drugs were administered together. In another study, co-administration of BKM120, a phosphoinositide 3-kinase inhibitor, with olaparib suppressed tumor growth more effectively in an *in vivo* prostate cancer model created with PC3 cells than in groups in which the drugs were administered separately (González-Billalabeitia et al., 2014). A randomized, open-label, phase 3 clinical trial evaluating the PARP-1 inhibitor olaparib in 4425 men with metastatic CRPC found that the olaparib-treated group had a longer duration of survival and a 66% reduction in disease progression compared to the enzalutamide or abiraterone (control) group. However, this study also included olaparib-related adverse symptoms such as nausea and anemia (de Bono et al., 2020b). A randomized, open-label phase 3 clinical trial was conducted to determine the effect of olaparib treatment on survival rates in patients with CRPC. For nearly 20 months, trial participants were given 300 mg of oliparib twice daily. The study found that patients with CRPC had a 31% higher life expectancy after starting olaparib (Hussain et al., 2020). The TOPARP-A clinical trial is a critical Phase II research looking at the effectiveness and safety of olaparib in CRPC patients. In this experiment, 50 patients received 400 mg olaparib twice daily. Approximately 33% of individuals treated with olaparib showed clinical improvement. Most responding individuals had BRCA2 mutations or abnormalities in other DNA repair genes. However, the most prominent adverse effects found during the trial were anemia and nausea (Mateo et al., 2015). Rucaparib is another PARPi used in mCRPC patients with mutations in BRCA1/2 and other DNA repair genes. Rucaparib supressess cancer cells proliferation by targeting DNA repair. In a study, rucaparib was shown to be effective in controlling disease in mCRPC patients with BRCA mutations. A reduction in PSA levels and tumour shrinkage were observed in patients participating in the study. On the other hand, side effects such as anemia, thrombocytopenia, and neutropenia have also been observed . Niraparib is another PARPi used in mCRPC patients with defects in the HRR pathway. Niraparib also inhibits DNA repair, inducing cancer cells to undergo apoptosis. In a study, niraparib was shown to be effective in mCRPC patients with HRR defects. While a reduction in PSA levels and tumour

shrinkage were observed in the patients participating in the study, adverse side-effects such as anaemia and neutropenia were also observed .

Considering the action mechanism of PARP-1 in DNA repair mechanism, it can be significant target for the treatment of CRPC. Looking ahead to literature, there are some FDA-approved drugs but most of them have harmful and unnegligible side effects. Therefore newly, target spesific and highly selective with has low side-effects drugs are required.

In our finished scientific research project (FIA-2021-3666) of Çanakkale Onsekiz Mart University, it was concluded that SELB-1 and SELB derivatives synthesized by Dr.Lukas Rycek from *Selaginella Pulvinata* have a high antiproliferative effect (IC_{50} : 5.9 μM for SELB-1 ; IC_{50} : 53,4 μM for SELB) ,and selectivity index (SI for SELB-1: 12,5 ; SI for SELB: 19) in prostate cancer cell line PC-3. Considering the results, we have hypothesized that SELB-1 and SELB compounds interact with prostate cancer-specific pathways and specific target molecules. To support this hypothesis, several databases were searched (Kegg pathway, Swiss Target Prediction, Ma'ayan Lab Computational Systems Biology) to identify pathways and target molecules (shown in Figure 2). *In silico* docking studies were carried out with the selected target molecules (PARP-1, PDE4D2, PDGFRA TLR4). As a results of docking analysis, the docking scores of SELB and SELB-1 have lowest bindig energy with PARP-1 (-10.7 and -10.3 kcal/mol, respectively). Furthermore, SELB-1 and SELB compounds showed more effective binding compared to reference molecule. Given the role of the PARP-1 enzyme in CRPC, it was hypothesised that SELB-1 could provide a scaffold/pharmacophore structure for the development of novel PARP inhibitors. In this thesis,in addition to SELB-1, nine other SELB-1-derived compounds were designed and evaluated for druggability by ADMET analyses. Cytotoxicity, proliferation and viability studies as well as PARP inhibition assays identified lead compounds. These lead compounds were then evaluated for their molecular mechanisms of action through *in silico* analyses. Molecular docking and dynamic studies provided detailed information on binding sites, key interactions and conformational changes in target proteins upon binding, thereby enhancing our understanding of their inhibitory potential. Overall, *in silico* approaches, provide insights into the conformational changes and dynamics of target-ligand

complexes and can be well integrated with experimental data to validate and refine hypotheses. This process increases the accuracy and reliability of conclusions.

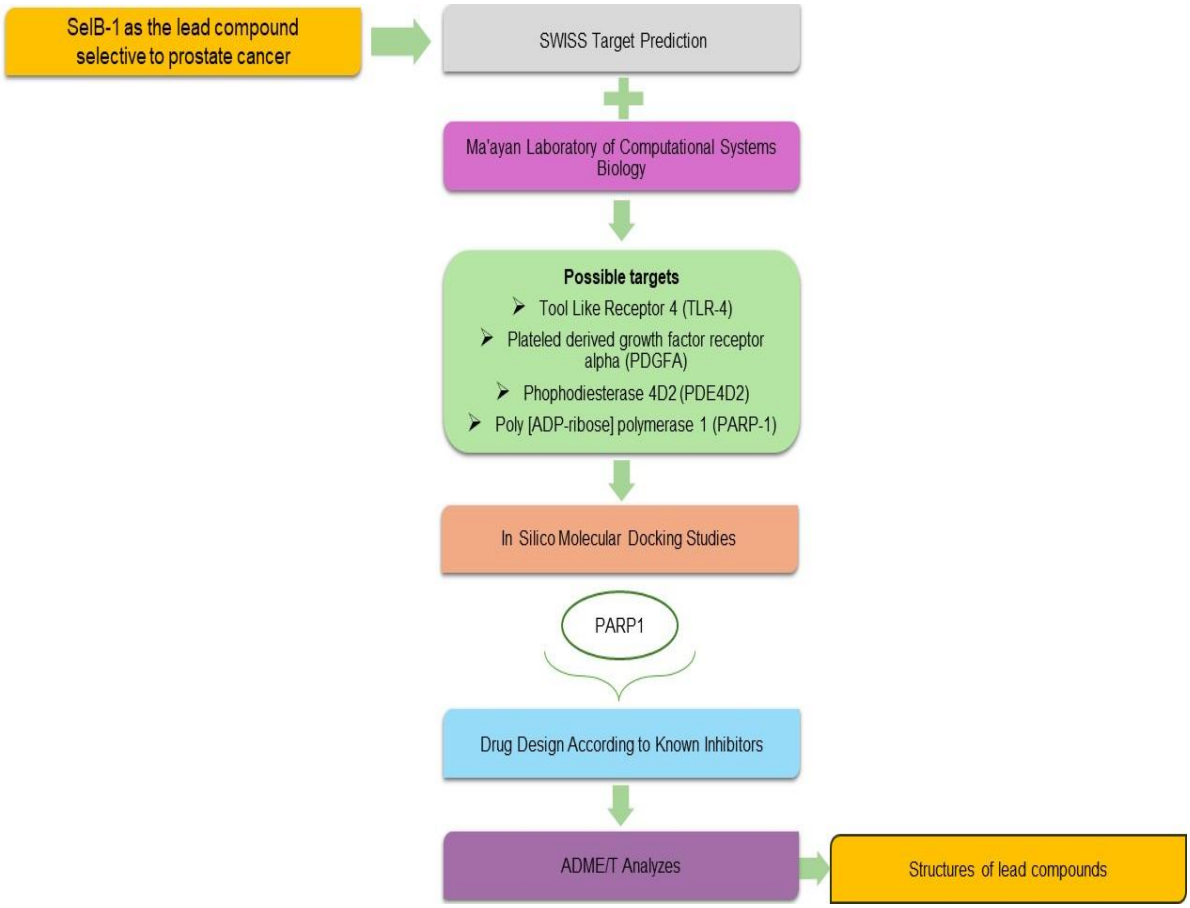


Figure 2. Flowchart of the target prediction.

1.3. *In silico* Molecular Dynamics and Docking Simulations

Today, many chemotherapeutic drugs with high side effects are used in the treatment of cancer. The development of new targeted drugs with low side effects plays an important role in treatment. Hence, the development and testing of drugs specific to particular targets, which can activate proangiogenic factors and promote angiogenesis and metastasis in tumors, is imperative. In this context, *in silico* techniques are frequently employed. Among the computational methods used in drug discovery, molecular dynamics and molecular docking simulations are widely utilized. Molecular dynamics (MD) simulations involve computationally studying the physical movements of atoms and molecules constituting proteins. These methods are extensively employed to obtain insights into the time-dependent

behavior, kinetics, and thermodynamics of proteins and other biological macromolecules. Such simulations offer detailed atomic-scale information about the dynamic structure of proteins and the interactions occurring within and between them. As a consequence, MD simulations have proven to be valuable tools for exploring the fundamental principles governing protein structure and function. The roots of MD methods can be traced back to the 1950s when they were originally developed within the theoretical physics community by Alder, Wainwright, and Rahman, focusing initially on simple atomic models. Over time, MD simulations were refined for more complex systems, culminating in the first empirical energy function-based simulation of a protein in 1976 (McCammon et al., 1977). The MD simulations are based on Newton's second law, which describes the relationship between force, mass, and acceleration. By initiating with the 3-D structure of a protein and assigning velocities to individual atoms, the forces and accelerations on each atom are computed iteratively to predict their subsequent positions. The MD trajectory, obtained by integrating the equations of motion, provides valuable data on the atomic positions, velocities, and single-point energy. Once these atomic properties are determined, the system's state can be extrapolated, either in the future or the past, utilizing high-performance computing and the fundamental MD algorithm.

Force potentials encompass intricate equations, which account for various molecular properties such as bond lengths, bond rotations, electrostatic interactions, and force/energy calculations. These potentials play a crucial role in MD simulations. In order to simulate different experimental conditions, MD methods employ periodic boundary conditions, where the central cubic box is replicated throughout all directions using a cubic grid. Ensuring accurate representation of experimental conditions is essential, and MD simulations allow for easy manipulation of physical parameters like pressure and temperature. Experimental setups typically involve constant temperature and volume (NVT ensemble) or constant pressure and temperature (NPT ensemble), with the latter being particularly suitable for simulating condensed phase systems and closely mimicking real-world conditions. Consequently, these conditions are taken into account when simulating proteins. When simulating at a constant energy, fluctuations in temperature occur due to the conversion between kinetic and potential energy components. Atomic velocities can be used to evaluate the instantaneous temperature. To replicate the natural environment of proteins

and cells, water molecules are added to the simulation. In MD simulations, there are two types of water models: implicit and explicit. Implicit water models represent solvents as a continuous solvated pattern instead of individual solvent molecules, and they are commonly employed to estimate the free energy of solute-solvent interactions in various biological processes. On the other hand, explicit water models consider solvents more explicitly and are used when a detailed understanding of solvent behavior is required or preferred. These models are derived from quantum mechanics, molecular mechanics, experimental data, or a combination thereof, and several different types have been developed. Among them, the TIP3P, TIP4P, TIP5P, SPC, and SPC/E water models are particularly popular (Adcock and McCammon, 2006).

After MD simulations, molecular docking technique is used to predict the preferred orientation and binding affinity of one molecule to a second when bound to each other to form a stable complex. Molecular docking is a computational method that predicts how small molecules (e.g., drug candidates) bind to biological targets (e.g., proteins, DNA). This method aims to model how a molecule can interact with another molecule, its binding site and binding affinity. Molecular docking is used as an important tool in drug discovery and development because it predicts how potential drug candidates will interact with biological targets, allowing less time and resources to be spent on laboratory experiments. The basic parameters of molecular docking are ligand, receptor, binding site, scoring function and search algorithms. Ligands are small molecules or molecules to be bound that are evaluated based on attributes such as chemical structure, polarity, flexibility, and conformation. The receptor is a big molecule or target molecule, often proteins or nucleic acids, whose binding location, structural flexibility, and surface features are investigated. The binding site is the ligand's unique binding location on the receptor, also known as the active or allosteric site. The scoring function is a mathematical model that determines the binding energy of the ligand to the receptor while accounting for numerous physicochemical interactions such as hydrogen bonds, hydrophobic interactions, and electrostatic interactions. Genetic algorithms, Monte Carlo simulations, and the Lamarckian genetic algorithm (LGA) are examples of search algorithms that are used to determine how the ligand would interact with the receptor best. Genetic algorithms use biological evolution principles to develop and optimize novel conformations. These algorithms employ genetic operations including mutation, recombination, and selection to determine the optimal ligand-receptor binding conformations. Monte Carlo simulations, on the other hand, produce random conformations,

calculate their energies, and choose the lowest energy conformation. This method can be used especially effectively in large search spaces. While, LGA generates new conformations using the evolutionary approach of genetic algorithms and enables these conformations to evolve evolutionarily before reaching higher energy levels. LGA is also suitable for flexible receptor and ligand modeling. The accuracy and efficiency of molecular docking are influenced by various factors working together. Interactions between biomolecules play a crucial role in the functioning of biological systems, influencing both normal and abnormal cellular behaviors as well as defense mechanisms against external pathogens. A detailed understanding of these interactions requires atomic-level insight into the structures of the linker interfaces. While many protein-protein complex structures have been identified through experimental methods like X-ray crystallography and made available in the Protein Data Bank, there remain complex structures that have yet to be fully characterized. Molecular docking techniques, which involve predicting complex structures by inputting two or more structures, are employed to address this gap in structural knowledge.

1.4. Aim of The Thesis

First of all, 9 different Selagibenzophenone B derivatives, which were designed by *in silico* techniques, were synthesized by our collaborator Dr. Lukas Ryczek and his team. The main purpose of the thesis is to conduct the *in vitro* preclinical experiments of these Selagibenzophenone B derivatives against CRPC cells and to elucidate the inhibitory properties of the compounds experimentally and *in silico* investigations (shown is Figure 3.). In line with the purpose, our goals are:

1. Determination of the effects of newly synthesized Selagibenzophenone B derivatives on cell viability in CRPC and healthy cell lines.
2. In the process following the determination of cytotoxic compounds, the anticancer action mechanisms of these compounds are investigated using different variables that are complementary and supportive of each other. Accordingly, *in vitro* wound healing and clonogenic assays will be performed. Cell death types will be determined in more detail by determining the levels of apoptotic genes using qPCR technique.
3. Determining the effect of PARP-1 inhibition on CRPC cells with enzyme inhibiton assay.

4. To carry out *in silico* modeling studies to elucidate the interaction mechanisms of compounds and PARP-1 protein simultaneously with the mechanism studies.

5. To investigate the druggability of the lead compounds through *in silico* ADME/T analysis

For the first time, when we tested our hypothesis that we put forward with the thesis;

-A new approach hypothesis based on inhibition of PARP-1 enzyme in the treatment of CRPC was tested. As it is known, there is no anticancer agent with high treatment success that is used effectively in the treatment of CRPC.

- Along with PARP-1 activities of synthesized molecules, their activities on various secondary anticancer mechanisms will be determined by preclinical *in vitro* studies. In this way, a multi- targeted study will be carried out by determining both the prostate cancer-specific target protein interactions of molecules. This approach increases the novelity of the thesis.

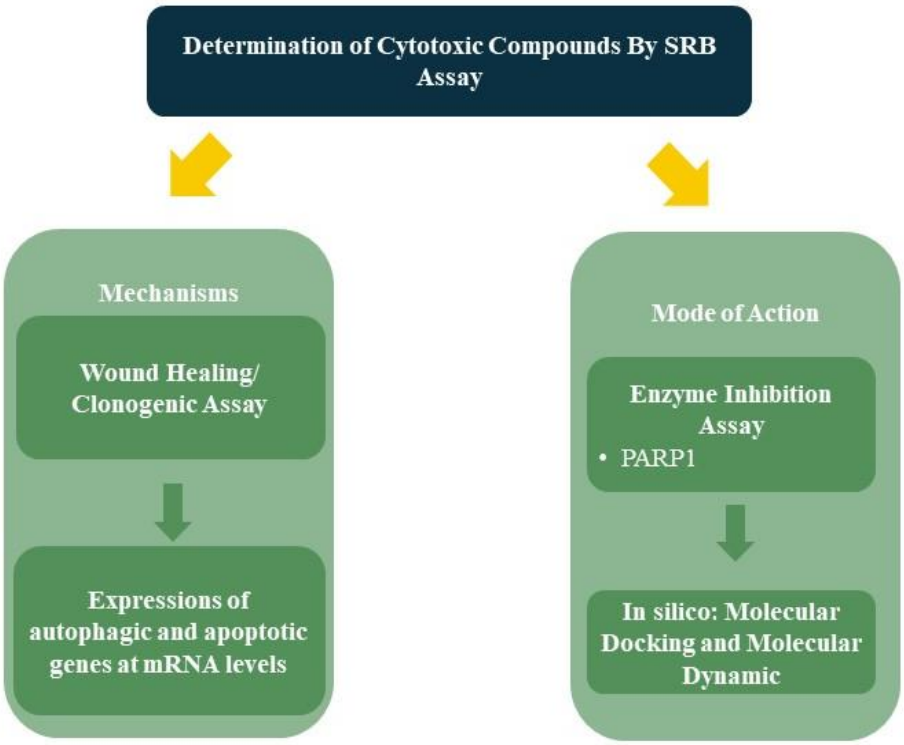


Figure 3. Flowchart of the study.

CHAPTER 2
PREVIOUS STUDIES

Selagibenzophenone B derivatives (SB2, SB3, SB4, SB5, SB6, SB7, SB8, SB9, and SB10) used in this study have not been examined within the scope of any scientific research project. Additionally, no studies have demonstrated the inhibitory effect of these compounds on the PARP-1 enzyme on the treatment of CRPC. However, studies about the CRPC, inhibition of the PARP-1 enzyme, and anticancer effects of Selagibenzophenone derivatives are explained below, individually.

The origins of the Selaginella plant date back 700 years. This herb is used in traditional Chinese medicine for the treatment of jaundice, gonorrhea, bleeding and acute hepatitis. Although the chemical contents of these plants have been studied since 1971. However, in 2014, isolation of Selaginpulvillin derivatives (AD), which has not been found in nature before and is therefore unique, was isolated and these unique compounds effectively reduced coxsackie virus B3 (CVB3) infection *in vitro* and *in vivo* (D. Yin et al., 2014). In another study conducted in the same year, the effect of these compounds on the activity of the PDE4D2 enzyme, which is a kind of biomarker in prostate cancer (Böttcher et al., 2016), was investigated. The results showed that these substances highly effectively inhibited the PDE4D2 enzyme, with IC_{50} values ranging from 0.11 to 0.26 μM (Liu et al., 2014).

Recently, Lapinskaite et al., studied the anticancer and antibacterial properties of newly synthesized Selagibenzophenone A (SA) derivatives. First, the drugs' effects on the PDE4 enzyme were assessed by measuring cyclic adenosine monophosphate (cAMP) release in HEK293 (human embryonic kidney cell line) cells. None of the substances blocked cAMP release, indicating PDE4 enzyme function. This result was surprising given the previously documented PDE4 inhibitory action of SA derivatives. Furthermore, the cytotoxic impact of these compounds was investigated using three distinct cancer and healthy cell lines. The compounds had a minor cytotoxic impact on the MCF-7 cell line, but a strong cytotoxic effect on the colon and prostate cancer cell lines. 4ca had the most effective cytotoxic impact on the HT-29 and PC3 cell lines (IC_{50} values of 11.9 and 7.8 μM, respectively). Furthermore, compound 4ba demonstrated the highest selectivity towards the

HT-29 cell line . In addition to cytotoxicity experiments, the compounds were examined for antibacterial activity on three different bacterial strands, and none of them had an antimicrobial impact (Lapinskaite et al., 2023).

In another study conducted by same group, newly synthesized Selagibenzophenone B derivatives exhibited promising effects on prostate cancer cells. The study investigated the dual topoisomerase I/II inhibition capacities of these newly synthesized SB derivatives and determined their secondary anticancer activities. Results indicated that the SelB-1 compound is selective to PC-3 cells, a CRPC cell line. The compound demonstrated an IC_{50} value of 5.9 μM and a selectivity index of 12.5, indicating a favorable comparison of cytotoxicity against healthy cells (Dönmez et al., 2024).

CHAPTER 3
MATERIALS AND METHODS

3.1 . Materials

3.1.1. Chemicals and Kits

All of the reagents that were used in the methods were listed in Table 1.

Table 1
Chemicals and kits with catalogue numbers.

Chemicals and Kits	Brand - Catalogue Number
Methanol	Sigma-Aldrich Chemical - 24229
Acetic Acid	Sigma-Aldrich Chemical - 1.00056.2500
Trypan blue solution	Sigma-Aldrich Chemical - T6146
Sodium pyruvate	Sigma-Aldrich Chemical - P5280
Dimethyl sulfoxide (DMSO)	Sigma-Aldrich Chemical - D2650
Sulforhodamine B sodium salt	Sigma-Aldrich Chemical - S 1402
Doxorubicin hydrochloride	Sigma-Aldrich Chemical - D2975000
L-Cysteine	Sigma-Aldrich Chemical - C7352
Trisma base	Sigma-Aldrich Chemical - T1503
Crystal Violet	Sigma-Aldrich Chemical - 548 62 9
RPMI-1640 MEDIUM	Sigma-Aldrich R8758-500ML
Dulbecco's Modified Eagle's Medium (DMEM)	Life Technolo ies Thermo Fisher Scientific - 12800017
Trypsin-EDTA	Life Technolo ies Thermo Fisher Scientific - 25200056
Fetal bovine serum (FBS)	Life Technolo ies Thermo Fisher Scientific - 10500064
Penicillin-streptomycin	Life Technolo ies Thermo Fisher Scientific - 15140122
Dimethyl sulfoxide (DMSO)	Santa Cruz Biotechnology - sc-358801
Dulbecco's PBS	Caisson laboratories - PBPOI
PARP Universal Colorimetric Assay Kit	RnD Systems - 4677-096-K
Hyrdochloric acid	Tekkim -7647-01-0

3.1.2. Equipments

All of the equipment and devices that were used in the methods were listed in Table 2.

Table 2

Equipment and devices with brand and model numbers.

Brand - Model	Equipment
BUCHI - V 300	Vacuum pump
Esco - CCL 170T 8	Cell culture CO2 incubator
Esco - Class II BSC	Biological safety cabinet
Hettich - Universal 320R	Standard centrifuge
Hettich - MIKRO 200R	Refrigerated Micro Centrifuge
TECAN - Infinite 200 PRO	Microplate reader
Scientific Industries - Genie 2	Vortex
Invitrogen - Qubit 4	Fhurometer
HANNA Instruments - HI 2211	pH meter
Thermo Fisher Scientific - Applied BiosystemsTM 7500	Real-Time PCR Systems
Bio-Rad - PowerPacTM Basic	Basic Power Supply
Cleaver Scientific - MS 120910874	Wide Midi Horizontal Electrophoresis System
Vilber Lourmat - QUATUM ST4 1100 26MX	Gel Documentation Imaging System
Bio-Rad - T100TM	Thermal Cycler
Beckman Coulter - Allegra X-15R	Refrigerated Centrifuge

3.2. Methods

3.2.1. Cell Culture Conditions

In this thesis, two castration-resistant prostate cancer cell lines and one healthy prostate cell line were used for the *in vitro* experiments. Growth conditions of the cells given below;

PC-3 (human castration-resistant prostate cancer cell line), DU145 (human castration-resistant prostate cancer cell line), and PNT1-A (human prostate epithelial cells) were cultured in a medium consisting of DMEM supplemented with 10% fetal bovine serum (FBS), 100 U/mL penicillin, and 100 μg/mL streptomycin. The cells were then maintained at 37°C in an environment with a humidified atmosphere containing 5% CO_2 and 95% air. These cell lines, PC-3, DU145, and PNT1-A, were utilized to assess the potential anticancer and antiproliferative properties of Selagibenzophenone B derivatives. Nine different

derivatives (SB-2, SB-3, SB-4, SB-5, SB-6, SB-7, SB-8, SB-9, and SB-10) were synthesized by our collaborator Dr. Lukas Rycek from Charles University, Czech Republic, shown in Figure 4.

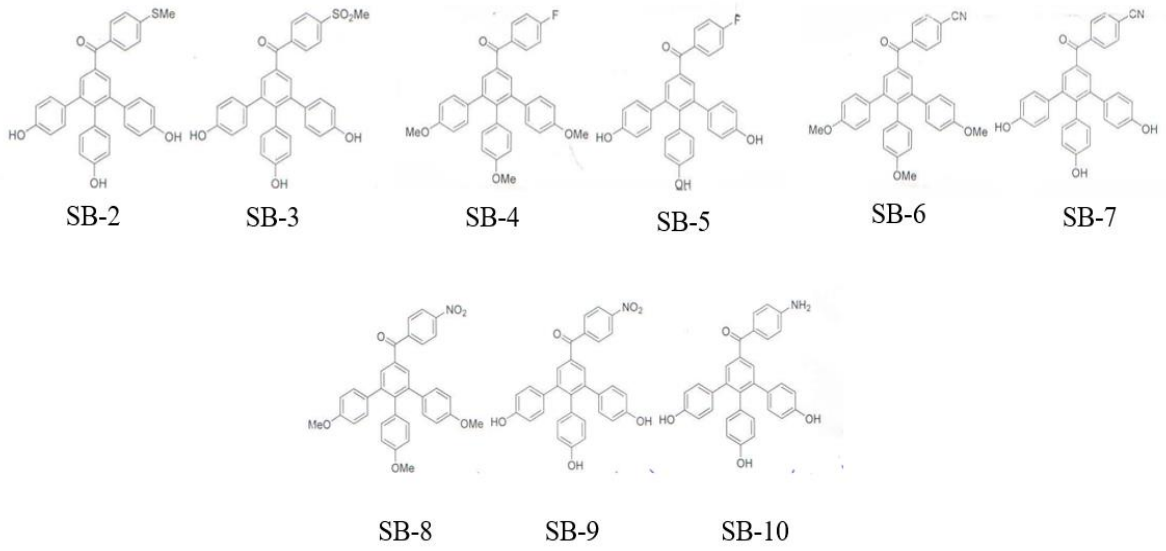


Figure 4. Structures of novel SB derivatives.

3.2.2. Cell Cytotoxicity Analyses

The effects of newly synthesized Selagibenzophenone B derivatives on cell viability was determined by the Sulforhodamine B (SRB) method. Doxorubicin was used as a positive control in all cell experiments. 96-well plates used for seeding cells at a concentration of $5x10^4$.Then, the compounds were applied in 3 repetitions at 6 different doses (1, 5, 10, 25, 50 and 100 µM) and incubated for 48 hours. After 48 hours, the medium was discarded from the wells, and 10% trichloroacetic acid (TCA) solution was added for the fixation and the plate incubated for 1 hour at +4°C. TCA was discarded from wells by washing 5 times with distilled water (dH_2O) and the plate was allowed to dry. Freshly prepared SRB dye solution (0.04 %) was added to each well and incubated for 30 minutes at room temperature. In the next step, the plate was washed 4 times with 1% acetic acid solution and left to dry. After the plate dried, 10 mM Tris-Base solution was added and incubated under constant shaking for 15 minutes. After this process, absorbance values were measured with the Tecan Infinite® 200 Pro device at 565 nanometers (nm). The dose range to be treated and IC_{50} values was determined by the statistical analysis program (Graphpad Prism 8).

3.2.3. Colony Formation Assay

Cells at the determined cell concentration (500 cells/well) were seeded into 6-well plates and incubated for 24 hours in growth conditions. Then, the cells were treated by selective compounds (SB-5, SB-7, SB-9 and SB-10) at determined doses by choosing 2 different doses according to IC_{50} values, generally IC_{50} and (2* IC_{50}). After incubation with compounds for 48 hours, the media was changed, and the cells were observed for a whole week. After a week of incubation, the media was withdrawn, and the cells were washed with PBS; The cells were fixed by adding 1 mL of 75% methanol + 25% acetic acid to each well. After 1 hour, the solution was discarded and 1 mL of 0.05% crystal violet dye was added to each well and incubated for 30 minutes at room temperature in the dark. The stained cells were washed 5 times with distilled water and images of the dried wells were taken. Colony formation (number of cells per unit area) was calculated with the ImageJ program.

3.2.4. Wound Healing Assay

DU145 and PC3 cells were seeded into 24-well plates at a concentration of $4.5x10^5$ and incubated for 24 hours. At the end of 24 hours, a wound was created by scratching the cells from the middle of the well with a pipette tip (200µL). Then, after washing each well with phosphate saline buffer solution (PBS), the media was changed and the selective compounds (SB-5, SB-7, SB-9 and SB-10) were applied to the cells at the determined doses (2 different doses are selected according to IC_{50} values, generally IC_{50} and (2* IC_{50}), in 2 repetitions and incubated for 48 hours. Images were taken at optimized incubation intervals (0-12-24-48 hours) with the software program (Launch ImageFocus 4 microscope integrated computer program) associated with the inverted microscope (Euromex). Statistical data analyzes (nanometers/day (nm/day)) completed with the help of ImageJ computer program.

3.2.5. Gene Expression Analysis

Total RNA from prostate cancer cells (PC-3 and DU145) was isolated using a Total® RNA Purification Plus Kit according to the manufacturer's protocol (Norgen Biotek, Canada). Thereafter, cDNA synthesis was carried out using a high-capacity cDNA reverse transcription kit (Applied Biosystems, Foster City, CA). A qPCR was conducted using an Applied Biosystems 7500 Real-Time PCR System with diluted cDNAs, specific TaqMan probes, and TaqMan PCR Master Mix. The comparative ΔΔCt method was applied to estimate the potency of selective compounds on mRNA levels. In an effort to establish the mRNA expression in relation to cellular processes of cell death induced by SB-5, SB-7, SB-9, and SB-10, the following genes were analyzed: LC3, Beclin-1, Bax, Bcl-2, and Caspase-3. In all the qPCR reactions, β-actin was also analyzed as the endogenous control.

3.2.6. PARP-1 Inhibition Assay

The PARP-1 inhibition assay was done according to the manufacturer's directions using HT Universal Colorimetric PARP Assay with Histone Coated Strip Wells. Rehydration of histones were made by adding 50 µl of 1X PARP buffer in each well, incubating them for at least 30 minutes at room temperature. After aspiration of the liquid, wells were added with 0.5 U/well of PARP-HSA enzyme with three different concentrations of test compounds and then mixed well again, followed by incubation for 10 minutes at room temperature. Thereafter, 25 µL of 1X PARP mix was added to all the wells, and the strip wells were incubated for 60 minutes at room temperature. The wells were then washed two times in 1X PBS + 0.1% Triton X-100 and two times in 1X PBS. Strep-HRP Working Solution was added to each well for 60 minutes at room temperature, and another washing step was performed. Finally, 50 µL of pre-warmed TACS-Sapphire colorimetric substrate was added to each well and incubated in darkness for 15 minutes. To the wells, 50 µL of a mixture containing 0.2 M HCl was added to stop the reaction. Finally, absorbance readings at 450 nm were taken using the Tecan Infinite® 200 PRO instrument. Once the experiment was over, three compounds (SB-7, SB-9 and SB-10) were selected as leads and the experiment was repeated at 6 different dose ranges in order to find out IC_{50} values for these compounds.

3.2.7. *In silico* Studies

Molecular Dynamics (MD) Simulations

MD simulations is one of the well-known techniques for understanding biological system dynamics, were conducted, enabling the exploration of molecular structures' dynamic nature (Carlson et al., 1999; Ozbil et al., 2012). First MD simulations on PARP-1 were run to obtain well-equilibrated protein structure. Thus, the x-ray crystal structure of PARP-1 (PDB ID: 3L3M) with resolution of 1 A, was fetched from the protein data bank. The simulations were performed in GROMACS 2018 program (M.J. Abraham, D. van der Spoel, E. Lindahl, B.Hess, 2018) employing the GROMOS96 54a7 force field (Schmid et al., 2011). Subsequently, protonation state of each titratable amino acid was determined based on prediction calculations from the PROPKA server (Søndergaard et al., 2011; Trott and Olson, 2010). Systems were then enclosed within simulation boxes and subjected to periodic boundary conditions. The PARP-1 protein was centered in a simulation box measuring 15 x 15 x 15 nanometers (nm). The box was filled with 22.275 SPC water molecules and 20 Na+ and 20 Cl- ions were added to neutralize the system. The system was first subjected to energy minimization and followed by 1 nanosecond (ns) long NVT (constant number of moles, volume and temperature), and NPT (constant number of moles, pressure and temperature) equilibration steps were applied to the system, in which the temperature was gradually increased (simulated annealing), respectively. Production MD simulations were performed using NPT ensemble. Constant 1.0 picosecond (ps)-1 bar pressure coupling and 0.1 ps - 298 K temperature coupling are paired as Protein and Non-Protein.

The protein system was subjected to 200 ns long MD simulations. As a result of MD simulations, the cluster structure was obtained from the time intervals between 150 and 200 ns. This cluster structure was obtained by clustering the structures with RMSD values within 3 nm using the clustering tool in the GROMACS 2018 program.

Molecular Docking Simulations

Molecular docking simulations were performed by AutoDock Vina 1.1.2 program (Trott and Olson, 2010). First of all, the lead compound (SB-7, which was chosen according to *in vitro* PARP-1 enzyme inhibition assay) was drawn by ChemDraw software and the reference molecule 3- aminobenzamide was taken from PubChem database as 3D form. Then, SB-7 was subjected to 1000 times energy minimization step by using YASARA with NOVA2 force field. After energy minimization of the compound, In the initial step, the cluster protein structure derived from the MD simulations was positioned within a grid box sized 70 Å X 70 Å X 70 Å, with a spacing of 1.00 Å. Subsequently, 20 poses were obtained and then clustered based on their binding mode and binding affinities. The protein-ligand structure resulting from the molecular docking simulations underwent classical MD simulations lasting 30 ns. These simulations were conducted using the GROMACS 2018 software with the same force field. For the PARP-1 protein-ligand complexes, a cubic box with dimensions of 15 × 15 × 15 nm was used and the same aforementioned conditions and procedures were followed.

At the end of the simulation, the protein-ligand binding free energy was then calculated using MM/GBSA by PRODIGY Ligand server. The program calculates protein-ligand binding free energy using the Molecular Mechanics/Generalized Born Surface Area (MM/GBSA) method.

3.2.8. Statictical Analyses

All statistical analyses were performed on GraphPad Prism 8 software. Data were obtained through biological and computer-based analyses. Results were represented as the standard error of mean ± (SEM). One-way analysis of variance (ANOVA) was used to make the comparison between control and treatment groups.

CHAPTER 4
RESULTS AND DISCUSSION

In this thesis, the effects of novel Selagibenzophenone B (SB) derivative compounds were investigated as their anticancer effects on castration-resistant prostate cancer cells, and PARP-1 inhibition capacity by *in vitro*, and *in silico* approaches.

4.1. Results of Biological Experiments

4.1.1. Determination of the Cytotoxic Effects of Novel SB Derivatives

The cytotoxic effects of SB derivatives were determined using the SRB method. The methodology entailed seeding cells into a 96-well plate at a density of 5×10^4 cells/well and incubating them at 37°C for 24 hours to allow for cell proliferation. Subsequently, the cells were treated with the compounds for a period of 48 hours. Following a 48-hour incubation period, the media was removed from the wells and the cells were incubated with a 10% trichloroacetic acid (TCA) solution at 4°C for one hour to facilitate fixation. Following a one-hour incubation period, the excess TCA was removed by washing the wells five times with water, after which they were left to dry. Once the wells had been rendered dry, they were incubated with 0.04% SRB for 30 minutes at room temperature in the absence of light. Thereafter, the wells were washed four times with a 1% acetic acid solution with a view to removing any excess SRB stain. After drying, the wells were incubated with 10% Tris-Base solution at room temperature for 20 minutes. Following this incubation period, the plate was read at 565 nm, and the requisite calculations were performed.

Initially, SB derivatives were treated on cells at six different doses (1 μM, 5 μM, 10 μM, 25 μM, 50 μM, 100 μM) to determine the IC_{50} of the compounds. The selectivity index (SI) was calculated separately for each prostate cancer cell line by dividing the IC_{50} results obtained in the healthy prostate epithelial cell line PNT1-A cells.

Table 3 presents the calculated IC_{50} and SI values for the 9 different derivatives for DU145, PC-3, and PNT1-A cells. Considering these results, compounds with an IC_{50} dose below 10 μM for both cancer cell lines and an SI value above 2 were selected as leads. The lead compounds are marked in red in the table (SB-5, SB-7, SB-9, and SB-10). According

to the results, the IC_{50} values of SB-5 for DU145, PC-3, and PNT1-A cells were determined to be 6.80, 7.06, and 14.41 μM, respectively. The SI values of SB-5 were calculated as 2.1 and 2.0, respectively. According to these calculations, SB-5 showed similar levels of effectiveness against both cancer cell lines, but the SI values were lower compared to other lead compounds, indicating relatively low selectivity against cancer cell lines. The IC_{50} values of SB-7 for DU145, PC-3, and PNT1-A cells were determined to be 7.32, 6.04, and 40.09 μM, respectively. The SI values of SB-7 were calculated as 5.48 and 6.64, respectively. These results indicate that SB-7 is particularly effective against the PC-3 cell line and has low toxicity to healthy cells, demonstrating good selectivity against cancer cells. The IC_{50} values of SB-9 for DU145, PC-3, and PNT1-A cells were determined to be 6.09, 9.88, and 38.66 μM, respectively. The SI values of SB-9 were calculated as 6.35 and 3.91, respectively. These results indicate that SB-9 is particularly effective against the DU145 cell line, with a high SI value observed in this cell line. The IC_{50} values of SB-10 for DU145, PC-3, and PNT1-A cells were determined to be 7.73, 7.56, and 67.14 μM, respectively. The SI values of SB-10 were calculated as 8.69 and 8.88, respectively. These results indicate that SB-10 shows similar levels of effectiveness against both cancer cell lines and has low toxicity to healthy cells. Additionally, when examining the SI values, it is seen that SB-10 shows high selectivity against cancer cells. According to the results, IC_{50} doses below 10 μM and SI values above 2 were found in the cancer cell lines, and with these criteria, four lead compounds (SB-5, SB-10, SB-7, and SB-9) were selected for further studies such as wound healing, colony formation capacity assessment, and apoptosis/autophagy gene analysis with IC_{50} and IC_{50}*2 doses.

Table 3
IC_{50} values and selectivity indexes of SB derivatives.

Compounds	Cell Line			Selectivity Indexes (SI)	
	DU145	PC-3	PNT1-A	DU145	PC-3
SB-2	14.6	9.42	47.15	3.23	5.01
SB-3	23.13	19.91	57.94	2.50	2.91
SB-4	>100	>100	>100	-	-
SB-5	6.80	7.06	14.41	2.12	2.04
SB-6	25.83	>100	>100	-	-
SB-7	7.32	6.04	40.09	5.48	6.64
SB-8	14.64	>100	>100	-	-
SB-9	6.09	9.88	38.66	6.35	3.91
SB-10	7,73	7,56	67,14	8,69	8,88

4.1.2. Effect of Lead Compounds on Colony Formation Capacity

The effect of lead compounds on colony formation capacity was examined using a colony formation assay based on crystal violet staining. According to the method, DU145 and PC-3 cells were seeded at a concentration of 500 cells/well, and the IC_{50} and 2x IC_{50} values of the compounds were applied to the cells. The cells were then incubated at 37°C in an incubator with 5% CO_2 and 75% humidity for about a week to allow for colony formation. After incubation, the cells were fixed by incubating them with a 75% methanol and 25% acetic acid solution at room temperature for 1 hour. Then, the cells were treated with 0.05% crystal violet stain for 30 minutes. Subsequently, photographs of each well were taken and analyzed using the ImageJ program.

The colony formation capacities of SB derivatives in DU145 cells are shown in Figure 5. As shown in Figure 4, doxorubicin which was used as a positive control at a 5 µM application dose, suppressed the colony formation capacity of the cells by approximately 97%. The results closest to the positive control were obtained for the SB-7 compound, with

suppression rates of around 72% for both doses (IC_{50} and 2x IC_{50}). The application of SB-5 moderately inhibited the colony formation of DU145 cells by approximately 27% and 30% at both doses, respectively; while the SB-10 compound showed a dose-dependent inhibition pattern with inhibition rates of 14% and 42% for the two different doses, respectively. The SB-9 compound inhibited the colony formation of DU145 cells in a dose-dependent manner .(The suppression rates for colony formation at IC_{50} and 2x IC_{50} for SB-9,were observed to be 4% and 17% ,respectively).

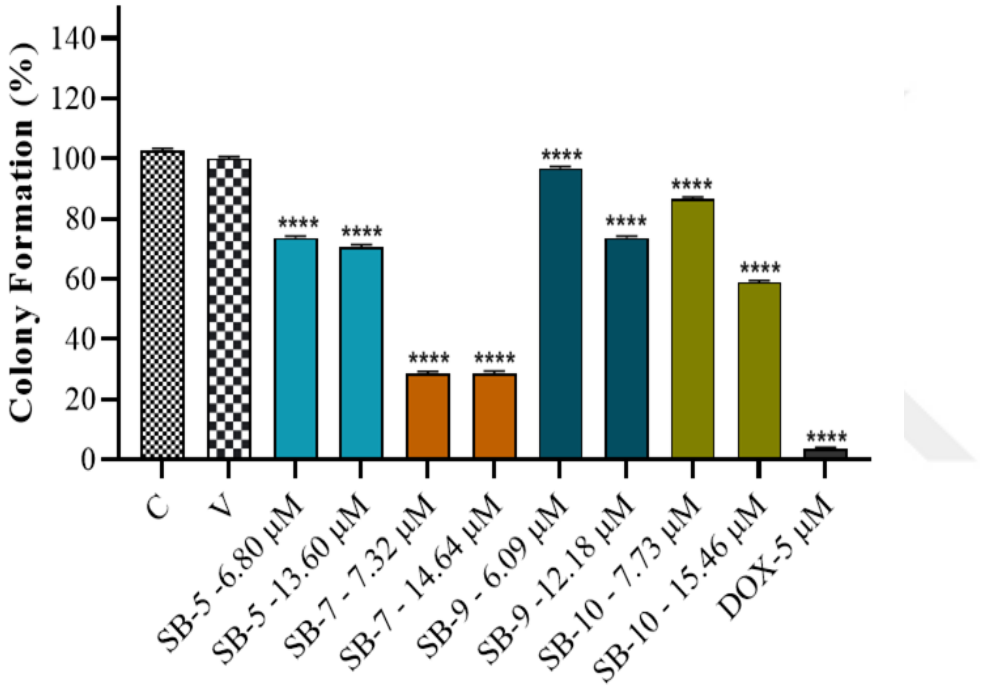


Figure 5. Colony formation capacity of selective SB derivatives on DU145 cells. Doxorubicin used as a positive control at 5 µM application dose. C: Control; V: DMSO. ****$p < 0.0001$.

The effect of SB derivative compounds on the colony formation capacity in PC-3 cells is shown in Figure 6. According to the results, doxorubicin, used as a positive control at 5 µM application dose, suppressed the colony formation capacity of the cells by approximately 95%. The results closest to the positive control were obtained for the SB-5, and SB-7 compounds. The application of SB-7 inhibited colony formation in a dose-dependent manner. SB-7 inhibited it by 37% and 83% at IC_{50} and IC_{50}*2 doses, respectively. For the SB-5 compound, an inhibition rate of 84% was observed at the IC_{50} dose, which was

higher than the IC_{50} dose of all other compounds, and an inhibition rate of 71% was observed at the 2x IC_{50} dose. In the SB-9 and SB-10 compounds, moderate suppression was observed with minimal differences between IC_{50} and 2x IC_{50} doses: 42% and 51% for SB-9, and 35% and 27% for SB-10, respectively.

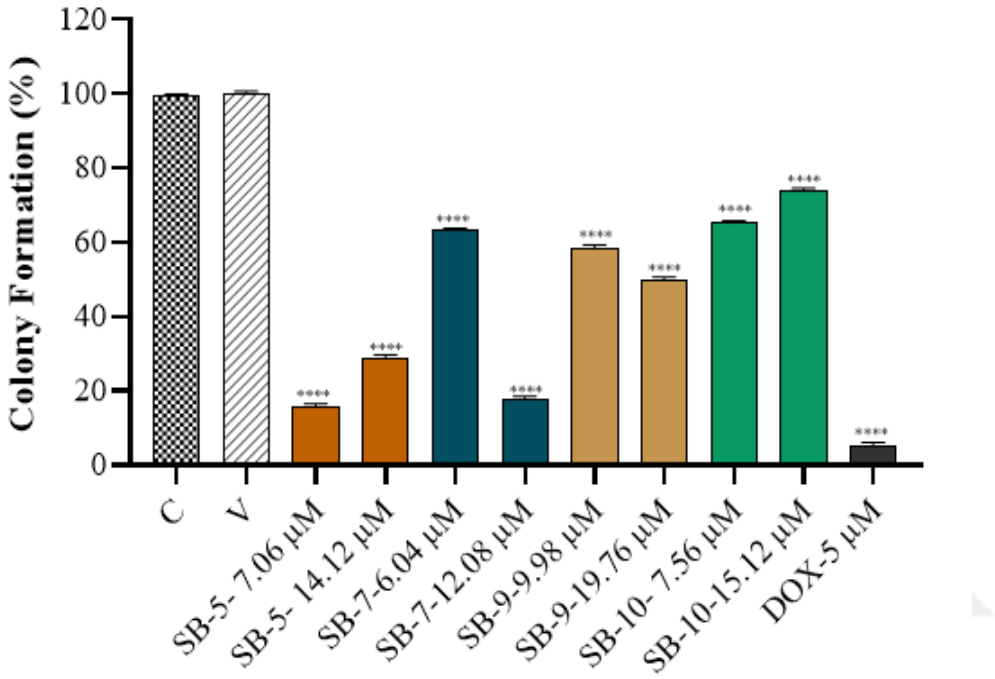


Figure 6. Colony formation capacity of selective SB derivatives on PC-3 cells. Doxorubicin used as a positive control at 5 µM application dose.C: Control; V: DMSO. ****$p < 0.0001$.

4.1.3. Effect of Lead Compounds on Wound Healing Capacity

The effect of SB derivative compounds on the wound healing capacity was examined using a wound healing assay with DU145 and PC-3 cells. The experiment is based on creating a scratch on the cell monolayer with a pipette tip. After creating the scratch, the cells were observed at four time points (0, 12, 24, and 48 hours) for their migration capacity. The wound healing results for DU145 cells are shown in Figure 7. According to the results, when the IC_{50} dose of SB-5 was applied, the wound healing rate was 18% at 48 hours in contrast to 0 hours; when the 2x IC_{50} dose was applied, the wound healing rate was 34% at 48 hours in contrast to 0 hours. In the negative control group, the wound healing rate was

80% at 48 hours in contrast to 0 hours, while in the doxorubicin-treated positive control group, the wound healing rate was 30% at 48 hours in contrast to 0 hours. At the IC_{50} dose of SB-5, a better result with a lower wound healing rate than the positive control was observed, while at the 2x IC_{50} dose, an effective result with a wound healing rate close to the positive control was observed. When the IC_{50} dose of SB-7 was applied, the wound healing rate was 20% at 48 hours in contrast to 0 hours; when the 2x IC_{50} dose was applied, the wound healing rate was 10% at 48 hours in contrast to 0 hours. In the negative control group, the wound healing rate was 80% at 48 hours in contrast to 0 hours, while in the doxorubicin-treated positive control group, the wound healing rate was 30% at 48 hours in contrast to 0 hours. At the IC_{50} dose of SB-7, a better result with a lower wound healing rate than the positive control was observed, while at the 2x IC_{50} dose, the most effective result with a much better wound healing rate than the positive control and other compounds was observed. When the IC_{50} dose of SB-9 was applied, the wound healing rate was 25% at 48 hours in contrast to 0 hours; when the 2x IC_{50} dose was applied, the wound healing rate was 20% at 48 hours in contrast to 0 hours. In the negative control group, the wound healing rate was 80% at 48 hours in contrast to 0 hours, while in the doxorubicin-treated positive control group, the wound healing rate was 30% at 48 hours in contrast to 0 hours. At the 2x IC_{50} dose of SB-9, a slightly better wound healing rate than the IC_{50} dose was observed, while at both IC_{50} and 2x IC_{50} doses, a good result with a lower wound healing rate than the positive control was observed. When the IC_{50} dose of SB-10 was applied, the wound healing rate was 37% at 48 hours in contrast to 0 hours; when the 2x IC_{50} dose was applied, the wound healing rate was 26% at 48 hours in contrast to 0 hours. In the negative control group, the wound healing rate was 80% at 48 hours in contrast to 0 hours, while in the doxorubicin-treated positive control group, the wound healing rate was 30% at 48 hours in contrast to 0 hours. At the IC_{50} dose of SB-10, a slightly worse result with a higher wound healing rate close to the positive control was observed, while at the 2x IC_{50} dose, a more effective result with a lower wound healing rate than the positive control was observed.

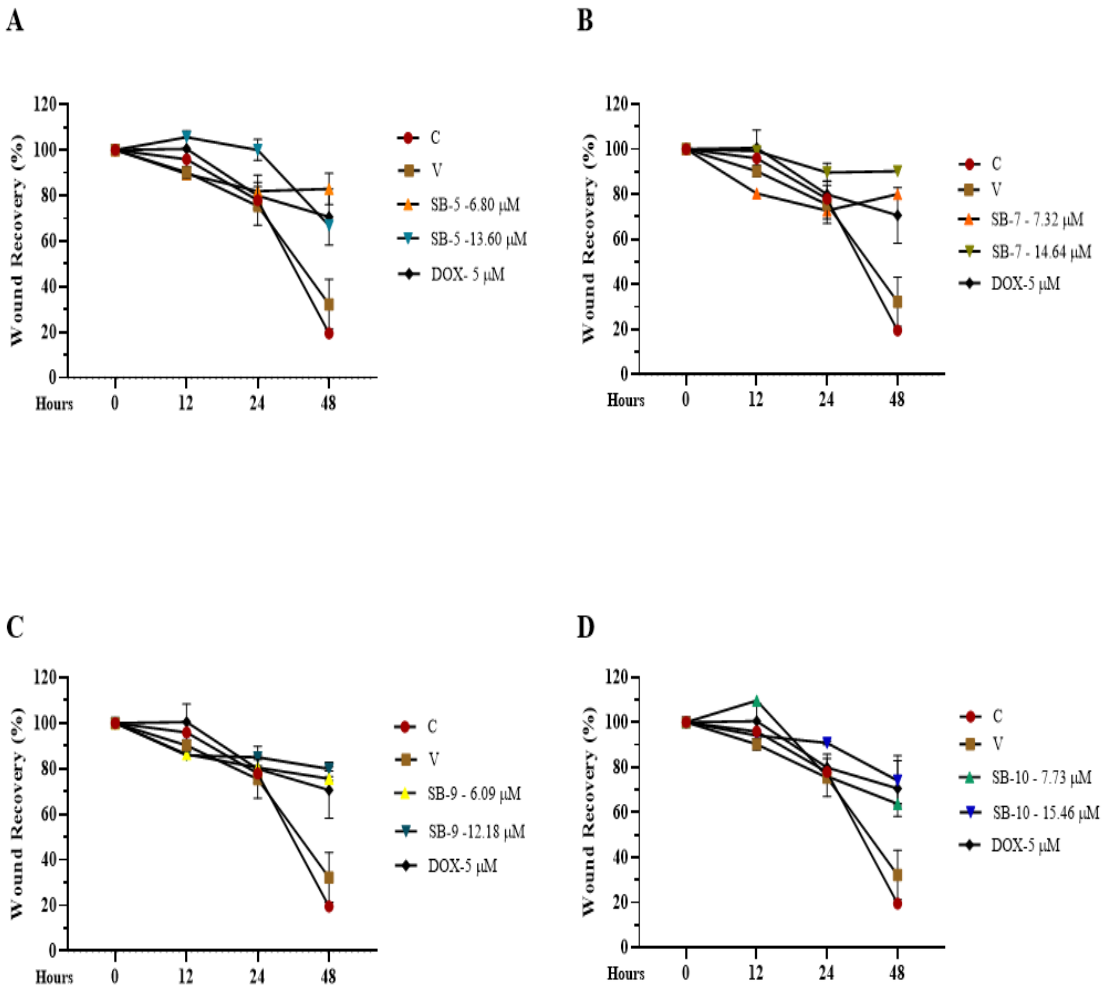


Figure 7. The effects of wound recovery capacities of the selective compounds on DU145 cells (A) SB-5, (B) SB-7, (C) SB-9, and (D) SB-10. Doxorubicin used as a positive control at 5 µM application dose.

Wound healing analyses in PC-3 cells are shown in Figure 8. According to the results, when the IC_{50} dose of SB-5 was applied, the wound healing rate was 52% at 48 hours in contrast to 0 hours; when the 2x IC_{50} dose was applied, the wound healing rate was 56% at 48 hours in contrast to 0 hours. In the negative control group, the wound healing rate was 61% at 48 hours in contrast to 0 hours, while in the doxorubicin-treated positive control group, no wound healing was observed. For SB-5, similar wound healing rates were observed at both IC_{50} and 2x IC_{50} doses, with both doses showing slightly less wound healing compared to the negative control, indicating a moderately good result. When the IC_{50} dose of SB-7 was applied, the wound healing rate was 45% at 48 hours in contrast to 0 hours; when the 2x IC_{50} dose was applied, the wound healing rate was 43% at 48 hours in contrast

to 0 hours. In the negative control group, the wound healing rate was 61% at 48 hours in contrast to 0 hours, while in the doxorubicin-treated positive control group, no wound healing was observed. For SB-7, similar wound healing rates were observed at both IC_{50} and 2x IC_{50} doses, with both doses showing much less wound healing compared to the negative control, indicating a good result. When the IC_{50} dose of SB-9 was applied, the wound healing rate was 40% at 48 hours in contrast to 0 hours; when the 2x IC_{50} dose was applied, the wound healing rate was 34% at 48 hours in contrast to 0 hours. In the negative control group, the wound healing rate was 61% at 48 hours in contrast to 0 hours, while in the doxorubicin-treated positive control group, no wound healing was observed. For SB-9, similar wound healing rates were observed at both IC_{50} and 2x IC_{50} doses, with both doses showing less wound healing compared to the negative control, indicating a good result. When the IC_{50} dose of SB-10 was applied, the wound healing rate was 41% at 48 hours in contrast to 0 hours; when the 2x IC_{50} dose was applied, the wound healing rate was 39% at 48 hours in contrast to 0 hours. In the negative control group, the wound healing rate was 61% at 48 hours in contrast to 0 hours, while in the doxorubicin-treated positive control group, no wound healing was observed. For SB-10, similar wound healing rates were observed at both IC_{50} and 2x IC_{50} doses, with both doses showing slightly less wound healing compared to the negative control, indicating a moderately good result.

In all compound applications, similar wound healing rates were observed for IC_{50} and 2x IC_{50} doses. When examining the results for SB-7, SB-9, and SB-10, all showed less wound healing compared to the negative control, but a higher wound healing rate compared to the positive control, indicating average results.

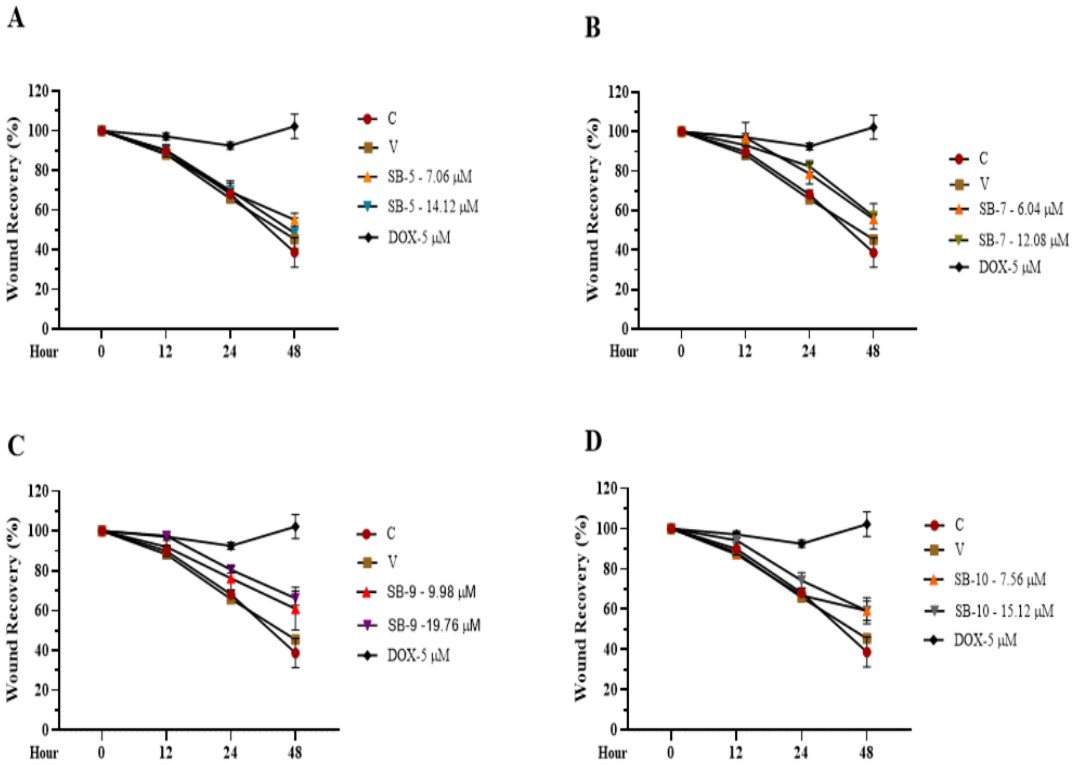


Figure 8. The effects of wound recovery capacities of the selective compounds on PC3 cells (A) SB-5, (B) SB-7, (C) SB-9, and (D) SB-10 . Doxorubicin used as a positive control at 5 µM application dose.

4.1.4. Effects of SB Derivatives on Relative mRNA Expression Levels of Apoptotic Genes

In this study, two cancer cell lines (DU145 and PC-3) were treated with selected lead compounds at their IC_{50} doses for 48 hours. Previous mRNA expression studies in our laboratory have shown that doubling the concentration of a cytotoxic compound (2x IC_{50}) can significantly affect gene expression results. The use of 2x IC_{50} leads to significantly higher cell death compared to IC_{50}, resulting in a considerable reduction in viable cell count, which can affect the quality and quantity of RNA isolated for gene expression analysis. Therefore, the IC_{50} dose was preferred for these analyses. Additionally, our laboratory studies have shown that doxorubicin at a 5 µM dose causes high toxicity. Therefore, doxorubicin was used as a positive control at a 1 µM dose for gene expression analyses.

Following the application, total RNA was isolated from the cells using the NORGEN Total RNA Purification Plus Kit, and cDNA synthesis was performed using the Applied Biosystems kit (Antika et al., 2023). The effects of the derivatives on apoptotic genes were then determined using specific TaqMan probes for Bax, Bcl-2, and Caspase-3. The effect of the compounds at IC_{50} doses on gene expression was determined by the comparative ΔΔCt method. To determine whether the compounds induce apoptosis in cells, expression levels of Bax, Bcl-2, and Caspase-3 were investigated. Additionally, a Bax/Bcl-2 ratio greater than 1 indicates that the compounds induce apoptosis. Therefore, Bax, Bcl-2, and Caspase-3 data for each compound in both cell lines were presented separately, along with Bax/Bcl-2 ratios in the figure.

Gene expression analyses in DU145 cells are shown in Figure 9. Regarding Bax gene expression results (Figure 9A), SB-9 by 1.18-fold; and SB-10 by 1.73-fold, while the positive control doxorubicin increased it by 1.04-fold. On the other hand, regarding Bcl-2 gene expression results (Figure 9B), SB-1 increased Bcl-2 gene expression by 1.05-fold; SB-5 by 1.38-fold; SB-7 by 1.51-fold; SB-9 by 1.38-fold; and SB-10 by 1.77-fold, while the positive control doxorubicin increased it by 1.04-fold. The increases in Bax and Bcl-2 expression levels gave similar results for each compound. Regarding Bax/Bcl-2 ratios (Figure 9C), the ratios were determined as 1.2 for SB-5, 1 for SB-7, 0.9 for SB-9, 1.1 for SB-10, and 1 for doxorubicin. Considering the results, SB derivatives increased the expression level of Bax gene in DU145 cells, while also increasing the expression levels of Bcl-2 gene at similar rates. Therefore, it is suggested that the compounds may not induce apoptosis through the Bax/Bcl-2 pathway. Regarding the expression levels of another apoptotic gene, Caspase-3 (Figure 9D), the results were 1.01 for SB-5, 0.79 for SB-7, 0.75 for SB-9, 0.91 for SB-10, and 0.65 for doxorubicin.

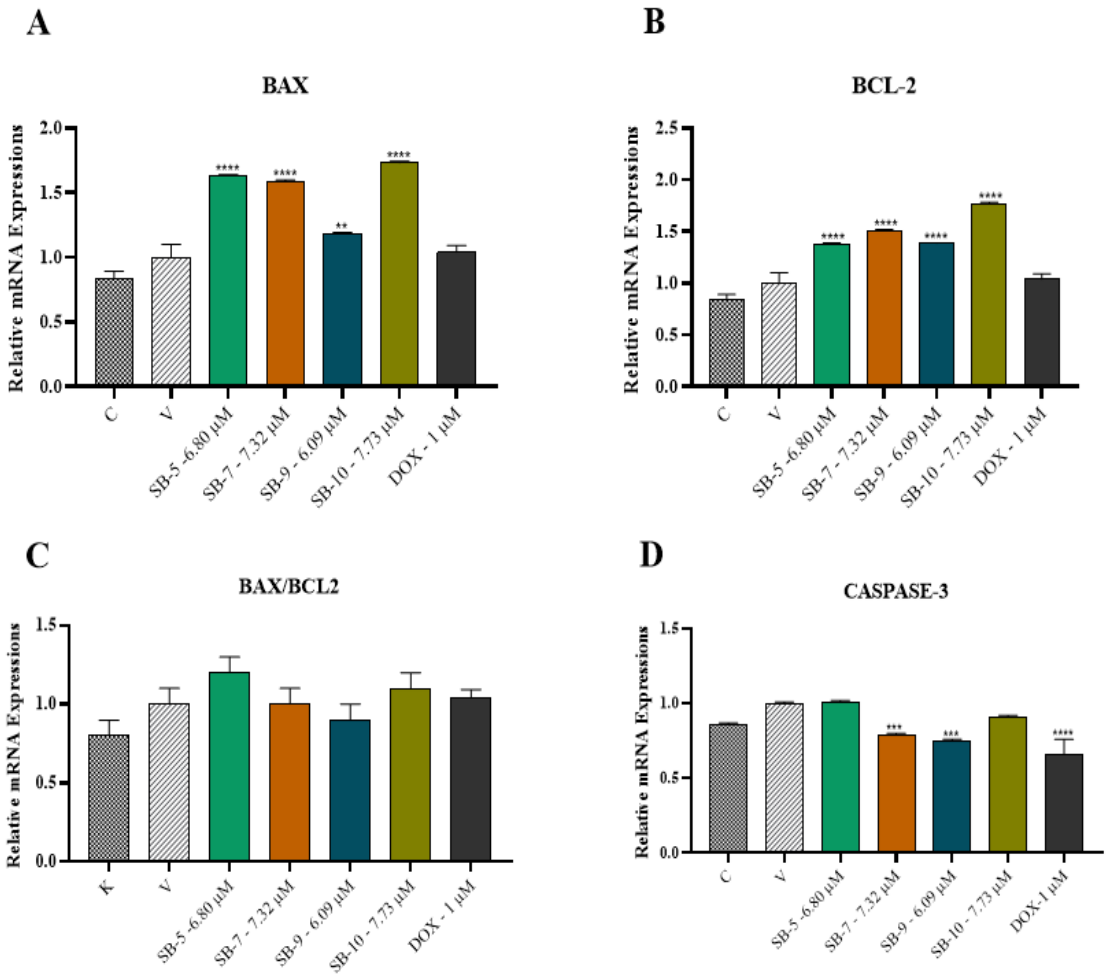


Figure 9. Relative mRNA expression levels of apoptotic genes on DU145 cells. Doxorubicin used as positive controls at 1 µM application dose. C:Control , V: DMSO. ****p < 0.001, ***p < 0.001 , **p < 0.01, *p < 0.05.

The results of the gene expression analyses investigating the effects of the derivatives on apoptotic genes in PC-3 cells are shown in Figure 10. Regarding Bax gene expression results (Figure 10A), SB-5 by 0.16-fold; SB-7 by 0.62-fold; SB-9 by 0.68-fold; and SB-10 by 0.56-fold. The positive control, doxorubicin, suppressed it by 0.26-fold. On the other hand, regarding Bcl-2 gene expression results (Figure 10B), SB-5 by 0.02-fold; SB-7 by 0.29-fold; and SB-9 by 0.26-fold, while SB-10 increased Bcl-2 gene expression by 1.55-fold. The positive control, doxorubicin, suppressed Bcl-2 expression by 0.26-fold. The changes in Bax and Bcl-2 expression levels gave similar results for each compound (Figure 10C). Regarding Bax/Bcl-2 ratios, the ratios were determined as 0.67 for SB-5, 0.53 for SB-7, 0.44 for SB-9, 0.29 for SB-10, and 1 for doxorubicin. Considering the results, SB derivatives did not cause significant differences in the expression levels of Bax and Bcl-2

genes in PC-3 cells. Therefore, similar to DU145 cells, it suggests that the compounds may not induce apoptosis through the Bax/Bcl-2 pathway. Regarding the expression levels of another apoptotic gene, Caspase-3 (Figure 10D), the results showed that SB-7 and SB-10 suppressed Caspase-3 gene expression by 0.15-fold, SB-7 by 0.01-fold, and SB-10 by 0.12-fold, while SB-5 increased Caspase-3 expression by 1.21-fold and SB-9 by 1.45-fold. Doxorubicin suppressed Caspase-3 expression by 0.34-fold. Based on the Bax, Bcl-2, and Caspase-3 gene expression results to determine whether the compounds induce apoptosis via the intrinsic pathway, it was found that the compounds did not have a significant effect on this pathway.

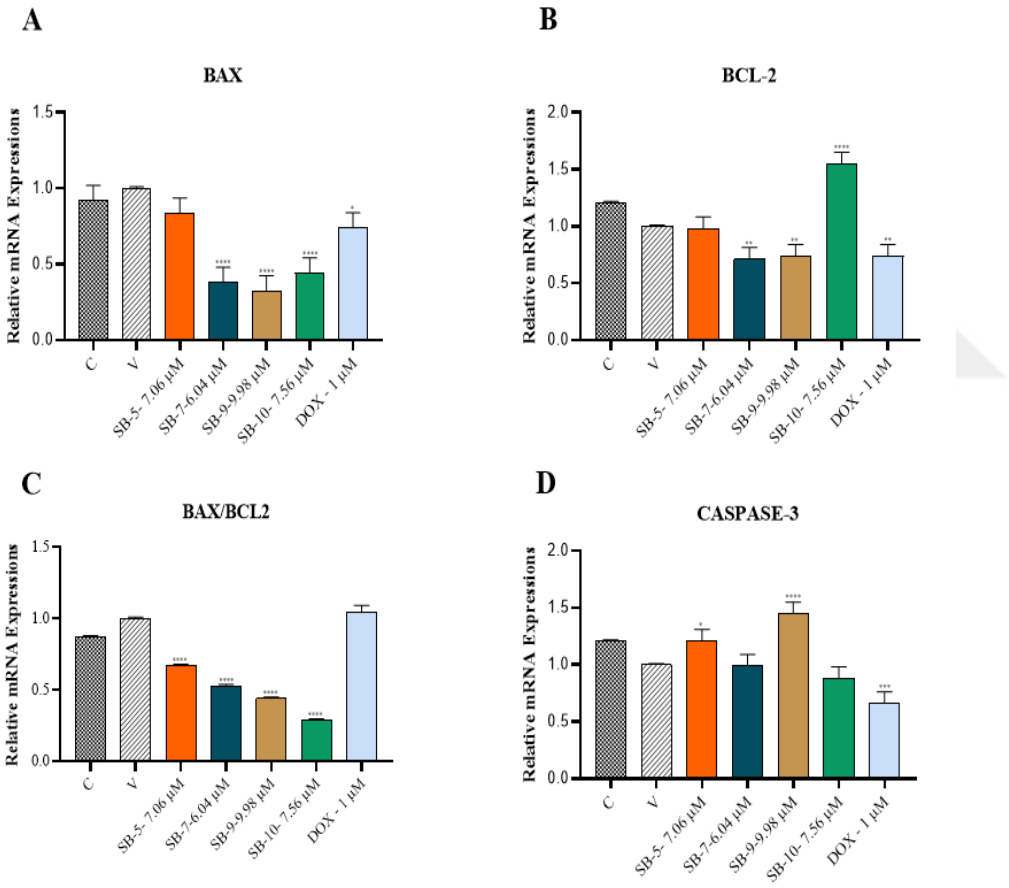


Figure 10. Relative mRNA expression levels of apoptotic genes on DU145 cells. Doxorubicin used as positive controls at 1 µM application dose. C:Control , V: DMSO. ****p < 0.001, ***p < 0.001 , **p < 0.01, *p < 0.05.

4.1.4. Effects of SB Derivatives on Relative mRNA Expression Levels of Autophagic Genes

To determine if the lead derivatives induce cell death through autophagy, qPCR was utilized. Two cancer cell lines (DU145 and PC-3) were treated with selected precursor compounds at IC_{50} doses for 48 hours. Total RNA was isolated from the cells using the NORGEN Total RNA Purification Plus Kit, and cDNA synthesis was performed using the Applied Biosystems kit. The effects of the derivatives on autophagic genes were determined using specific TaqMan probes for LC3 and Beclin-1. The gene expression effects at IC_{50} doses were determined using the comparative ΔΔCt method. LC3 is critical for the formation and elongation of the autophagosome membrane and is a significant marker of autophagic activity, while Beclin-1 initiates the autophagy process and regulates autophagic vesicle formation as a central component of a protein complex (Kabeya et al., 2000; Liang et al., 1998). Thus, the expression of these two genes plays crucial roles in the autophagic cell death pathway.

Gene expression analyses performed on DU145 cells are shown in Figure 11. For LC3 gene expression (Figure 11A), SB-5 increased expression levels by 1.65-fold, SB-7 by 1.83-fold, SB-9 by 1.8-fold, and SB-10 by 1.83-fold. The positive control, doxorubicin, increased LC3 gene expression by 1.16-fold. For Beclin-1 gene expression (Figure 11B), SB-5 increased expression levels by 1.3-fold, SB-7 by 2.75-fold, SB-9 by 1.95-fold, and SB-10 by 2.28-fold. Doxorubicin increased Beclin-1 gene expression by 1.24-fold. These results suggest that especially SB-7 significantly increases the expression levels of both LC3 and Beclin-1, indicating that SB-7 may induce autophagy in DU145 cells.

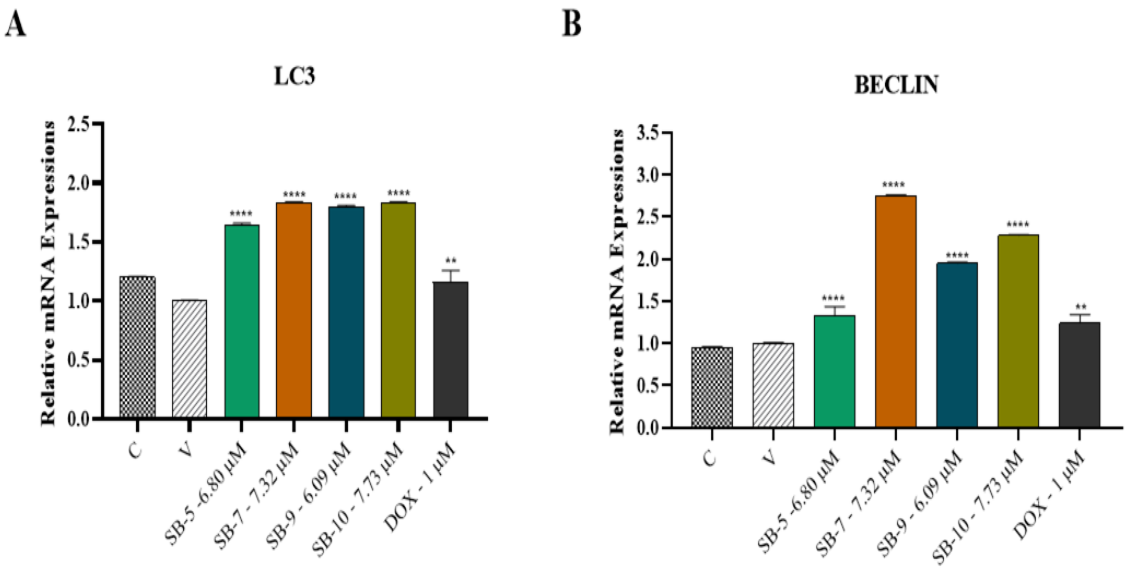


Figure 11. Relative mRNA expression levels of autophagic genes on DU145 cells. Doxorubicin used as positive controls at 1 µM application dose. C:Control , V: DMSO. ****p < 0.001, ***p < 0.001 , **p < 0.01, *p < 0.05.

The gene expression analyses performed with PC-3 cells are shown in Figure 12. Looking at the expression results of the LC3 gene (Figure 12A), the SB-5 compound suppressed LC3 gene expression levels by by 0.26; the SB-7 compound by 0.39; the SB-9 compound by 0.42; and the SB-10 compound by 0.35. The positive control, doxorubicin, increased the expression by 1.16-fold. When we look at the expression levels of another autophagic gene, Beclin (Figure 12B), the SB-5 compound suppressed Beclin gene expression levels by 0.16; the SB-7 compound by 0.48; the SB-9 compound by 0.42; and the SB-10 compound by 0.27-fold. The positive control, doxorubicin, increased the expression by 1.24-fold. Considering the results, it suggests that SB-derived compounds do not have significant autophagic activity in PC-3 cells.

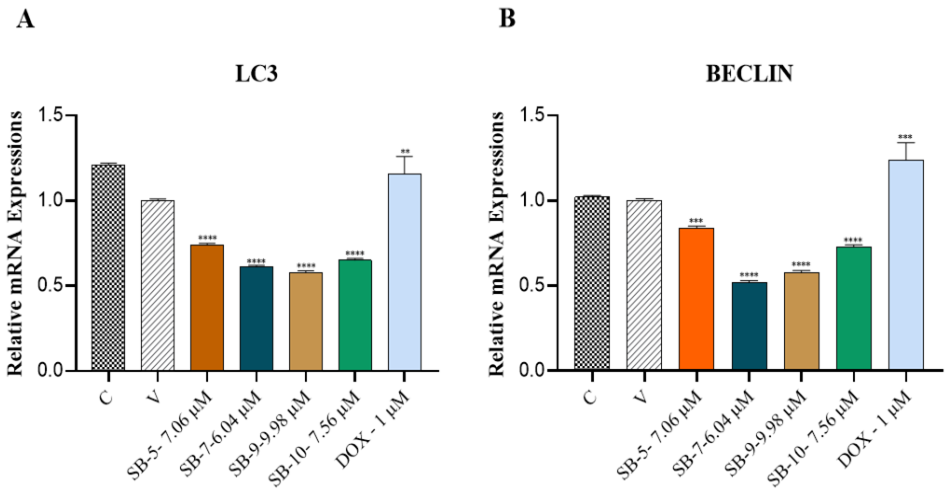


Figure 12. Relative mRNA expression levels of autophagic genes on PC-3 cells. Doxorubicin used as positive controls at 1 µM application dose. C:Control , V: DMSO. ****p < 0.001, ***p < 0.001 , **p < 0.01, *p < 0.05.

4.1.5. PARP-1 Inhibition Capacities of The Selective SB Derivatives

To evaluates the inhibition of PARP-1 enzyme activity , the HT Universal Colorimetric PARP Assay with histone-coated strip wells used. Initially, histones were rehydrated with 1X PARP buffer. After removing the buffer, different concentrations of the test compounds, along with PARP-HSA enzyme, were added and incubated. Subsequently, 1X PARP mix was introduced and incubated for 60 minutes. The wells were washed with PBS + 0.1% Triton X-100 solution and PBS before adding Strep-HRP Working Solution for a 60-minute incubation. Following another wash, pre-warmed TACS-Sapphire colorimetric substrate was added and incubated in darkness for 15 minutes. The reaction was stopped with 0.2 M HCl, and absorbance was measured at 450 nm.

Firstly, selected compounds (SB-5, SB-7, SB-9, and SB-10) were evaluated for their inhibitory activity against PARP-1 at concentrations of 1, 10, and 100 µM. The commercially available 3-aminobenzamide (3-AB) compound, provided as a reference molecule, was assessed at the same doses as the test compounds in the enzyme inhibition study. The results showed in Figure 13. The results demonstrated that, at a 100 µM concentration, SB-5

exhibited a 30% inhibition , SB-7 showed a 22% inhibition, SB-10 inhibited PARP-1 activity by 20%, and SB-9 achieved a 15% inhibition. Due to its comparatively lower inhibition effect, SB-9 was excluded from subsequent screening studies. The reference compound 3-AB displayed a 32% inhibition at 1 µM, 72% at 10 µM, and 98% at 100 µM. Although the selected compounds did not achieve inhibition levels comparable to 3-AB, those with inhibition rates exceeding 20% were further evaluated at higher doses (250, 500, 1000, and 2000 µM) to determine the best inhibiiton doses of the compounds.

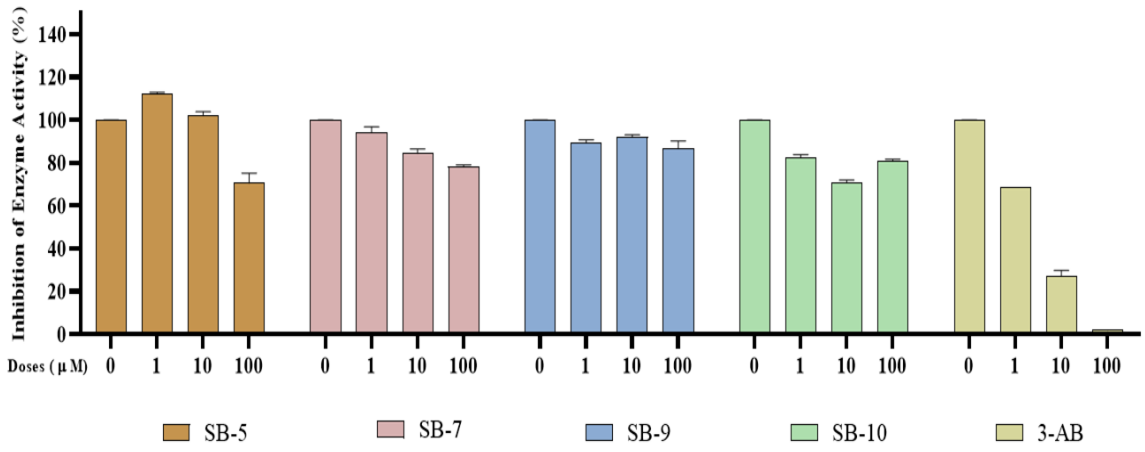


Figure 13. PARP-1 inhibition capacities of the selective SB derivatives at 1-10-100 µM doses.

The SB-5, SB-7, and SB-10 compounds were screened at doses of 250, 500, 1000, and 2000 µM, with the results depicted in Figure 14. SB-5 exhibited 20% inhibition at 250 µM, 18% at 500 µM, 30% at 1000 µM, and 42% at 2000 µM. SB-7 demonstrated 12% inhibition at 250 µM, 31% at 500 µM, 48% at 1000 µM, and 54% at 2000 µM. SB-10 showed 31% inhibition at 250 µM, 40% at 500 µM, 42% at 1000 µM, and 53% at 2000 µM.

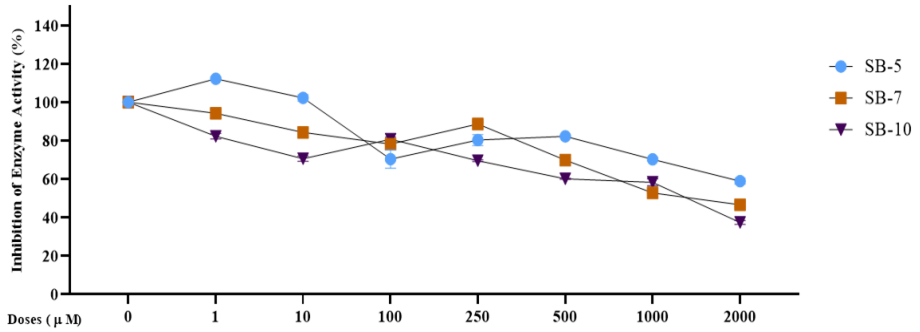


Figure 14. PARP-1 inihibiton capacities of the SB-5, SB-7 and SB-10 compounds at 1-2000 µM doses.

After screening the inhibition capacities of the derivatives, IC_{50} values were determined as presented in Table.4 The IC_{50} values were determined to be 2.69 µM for the reference compound 3-AB, 4.9 mM for SB-5, 1.8 mM for SB-7, 2 mM for SB-9, and 1.9 mM for SB-10.

Table 4

PARP-1 IC_{50} values of the selective SB derivatives.

Compounds	**IC_{50}**
SB-5	4.9 mM
SB-7	1.8 mM
SB-9	2 mM
SB-10	1.9 mM
3-AB	2.69 µM

Based on these findings, compound SB-7 was identified as the most potent precursor compound and further investigations were conducted using MD and molecular docking analyses. These computational studies aimed to provide insight into the compound's interaction with its molecular target, offering a deeper understanding of its mechanism of action.

4.2. Results of *In silico* Studies

After conducting biological research, MD simulations and molecular docking analyses were performed with the selected SB-7 compound and the reference compound 3-aminobenzamide.

4.2.1. MD Simulations of PARP-1 Protein Structure

Firstly, the PARP-1 X-ray crystal structure, created by Thomas et al., was obtained from the PDB server with the code 3L3M. The A927929 ligand and water molecules were removed from the structure using the YASARA Structure program. The resulting clean structure was subjected to MD simulations to achieve a well-balanced protein structure. The clean protein structure was then uploaded to the PROPKA server to determine the protonation states of titratable amino acids, revealing that each amino acid had the required pKa value. Subsequent MD simulations were conducted using the GROMACS 2018 program on the TRUBA-ULAKBİM server, employing the Gromos 54A7 force field. The PARP-1 protein structure was placed in a 15 x 15 x 15 nm simulation box, which was then filled with 22275 SPC water molecules to simulate the biological environment. To neutralize the system, 20 Na+ and 20 Cl- ions were added. The system, containing water, ions, and protein, underwent energy minimization for 1000 ns. Following energy minimization, the system was equilibrated at a constant temperature (298 K) through 100 ns NVT steps and then equilibrated at the specified pressure and temperature through NPT steps. The system, designed to reflect the biological experimental conditions, was subsequently subjected to a 200 ns MD simulation. After MD simulations RMSD (Root Mean Square Deviation) value of the protein structure was determined. RMSD is a metric used to measure the average atomic deviation between two structures in MD simulations or structural biology studies.The

RMSD analysis, shown in Figure 15, indicated that the protein structure was balanced between 150-200 ns MD simulation.

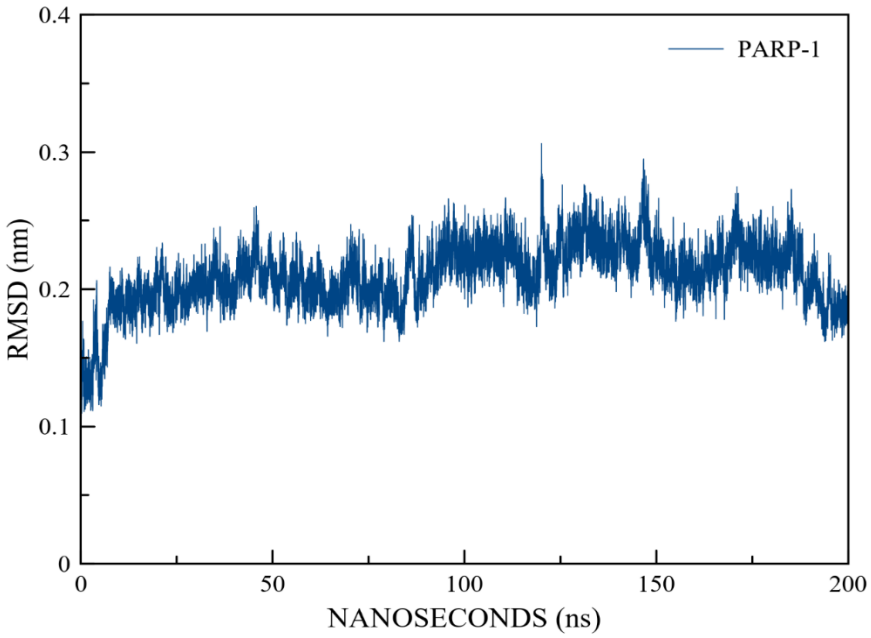


Figure 15. RMSD values of the PARP-1 protein structure throughout 200 ns long MD simulation.

Based on this result, a cluster structure from the 150-200 ns interval was selected for further molecular docking analyses (Figure 16).

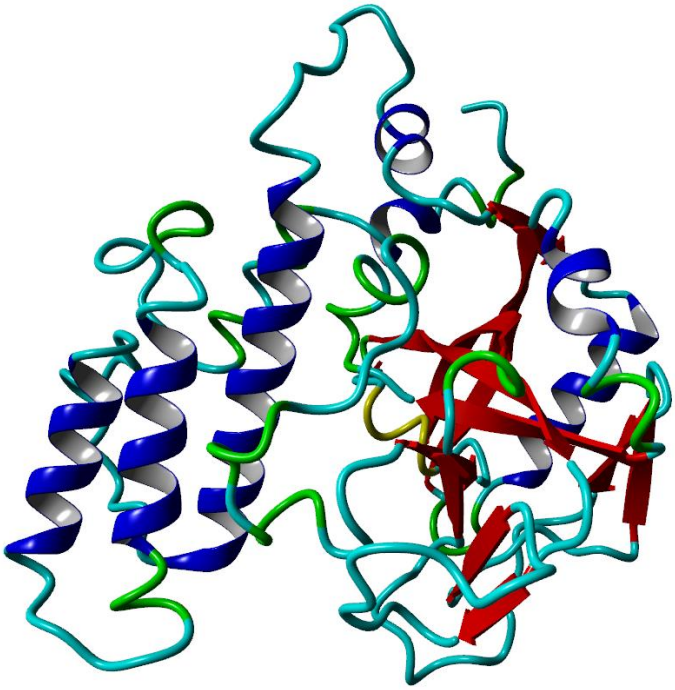


Figure 16. Cluster PARP-1 structure obtained from 150-200 ns time intervals.

4.2.2. Molecular Docking Studies

Prior to molecular docking simulation, the SB-7 compound was drawn using ChemDraw and subjected to 1000 energy minimization cycles with the NOVA2 force field in the YASARA Structure program, structures of SB-7 and 3-AB were shwon in Figure 17 as 2-D and 3-D forms.

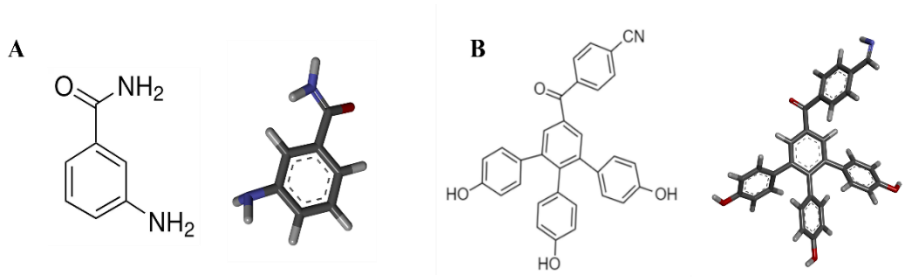


Figure 17. 2-D and 3-D structures of (A) 3- AB, and (B) SB-7 ligands.

After preparing the ligand, the protein and ligand (SB-7) were placed in a 70 x 70 x 70 nm grid box using the Autodock Vina 1.1.2 program. Molecular docking steps were performed 20 times in a box of dimensions X: -0.009564 , Y: 0.089770, Z: -0.209040. The same docking protocol was applied to the 3-AB reference compound used in the biological experiment. The binding energies obtained from molecular docking are shown in Table.5. The SB-7 compound demonstrated a significantly lower binding energy than the reference molecule, 3-AB (-9.9 and -5.8, respectively).

Table 5
Binding affinities of the protein-ligands after molecular docking simulations.

Compounds	**Binding Affinity (kcal/mol)**
SB-7	-9.9
3-AMINOBENZAMIDE (Control Ligand)	-5.8

Interactions between the compounds and PARP-1 after molecular docking and MD simulations were visualized by Discovery Studio 2021 Client software (BIOVIA, Dassault Systeèmes, Discovery Studio Client, San Diego: Dassault Systeèmes, 2021). The interactions between the protein and ligands are illustrated in Figure 18. As shown in Figure 18-A, the 3-AB compound formed hydrogen bonds with amino acids Lys137, Leu212, Ser213 and Leu216, as well as a π-alkyl interactions with Leu338 and a salt bridge with

Glu183. In contrast, Figure 18-B shows shows the interactions between the SB-7 compound and amino acids. These include hydrogen bonds with Gly202 and Ala237, a π -cation with Lys242, a π -anion with Glu327, and pi-pi-T-shaped bonds with Tyr228 and Tyr235.

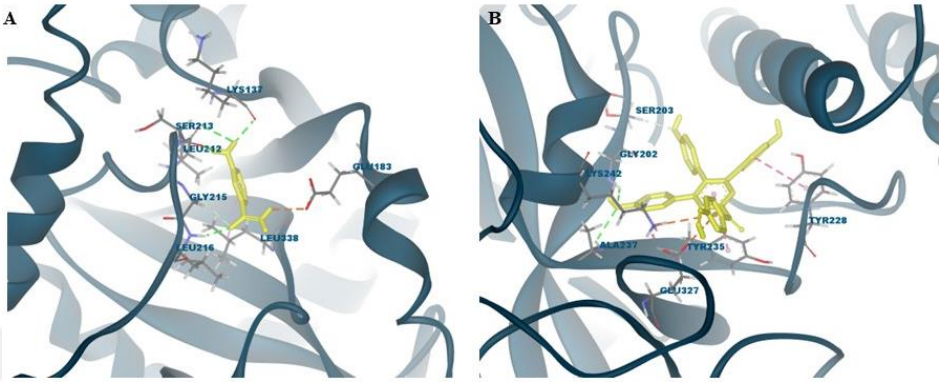


Figure 18. Representations of the interactions between PARP-1, and (A) 3-AB, (B) SB-7 after molecular docking.

4.2.3. MD Simulations After Molecular Docking Studies

Following molecular docking analysis, the pose with the best binding energy was selected, and the molecule was subjected to further MD simulations. Protein-ligand MD simulations were conducted for 30 ns for both the SB-7 and the reference compound 3-AB. After MD simulations RMSD values of the compounds were determined as shown in Figure 19. According to the RMSD results, for both 3-AB and SB-7, protein and ligand structures were balanced between 20-30 ns time intervals.

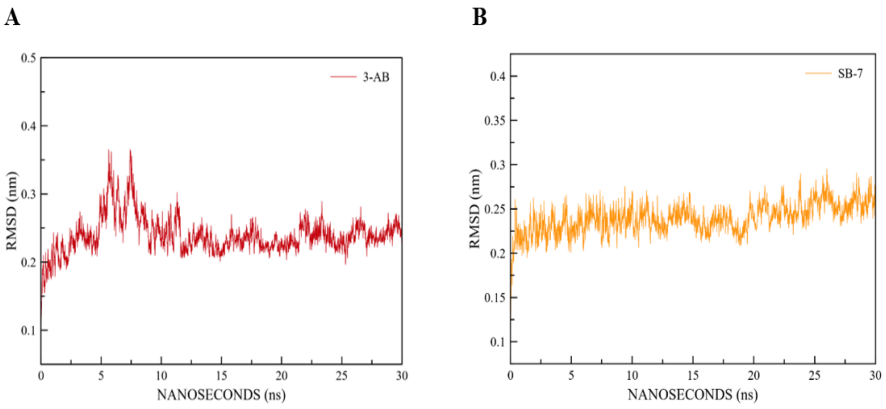


Figure 19. RMSD values of the protein with 3-AB (A), and SB-7 (B).

To determine the binding energies of the ligands, every poses between 20 and 30 ns were taken individually, and the binding energies were calculated using PRODIGY-Ligand server. Results were shown in Table.6. Results indicated that 3-AB molecule bound to PARP-1 with a binding energy as-5.8 kcal/mol while the lead compound SB-7 bound to PARP-1 with a lower binding energy as -11.8 kcal/mol.

Table 6

Binding energies of the 3-AB and SB-7 compounds after protein-ligand MD simulations.

Compounds	**Binding Energy (kcal/mol)**
SB-7	-11.8
3-AB(Control Ligand)	-5.8

The interactions between the protein and ligands after MD simulations are illustrated in Figure 20. As shown in Figure 20-A, the 3-AB compound formed hydrogen bonds with amino acids Arg180, Gly182, and Gly183. In contrast, Figure 20-B shows shows the interactions between the SB-7 compound and amino acids. These include hydrogen bonds with Gln98, Gly202, and Tyr235, a π-π stacked bonds with Gly227, Tyr228, and Tr246.

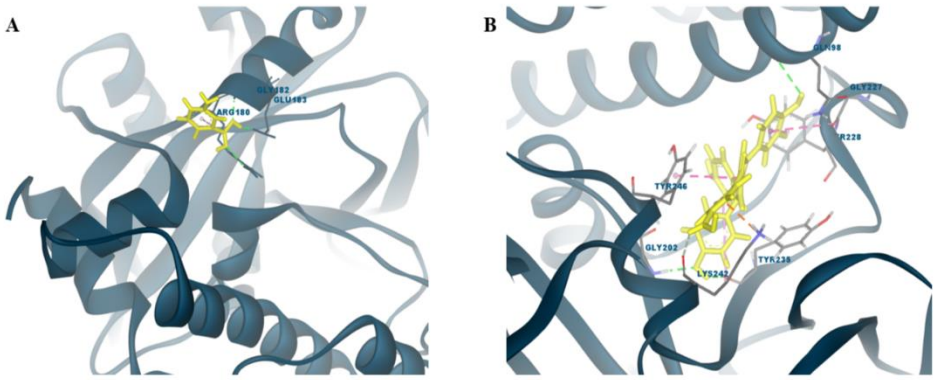


Figure 20. Representations of the interactions between PARP-1, and (A) 3-AB, (B) SB-7 after MD simulations.

4.2.4. Root-Mean Square Fluctuation (RMSF) Analysis

RMSF analysis was performed to determine the structural changes of amino acids and flexibility of specific regions in the protein depending on time. RMSF analysis of 3-AB ligand and PARP-1 protein was shown in Figure 21. The results show that there is no significant energy change between residues 150-200 where the 3-AB ligand is bound. This indicates that the 3-AB ligand remains fixed in its binding site.

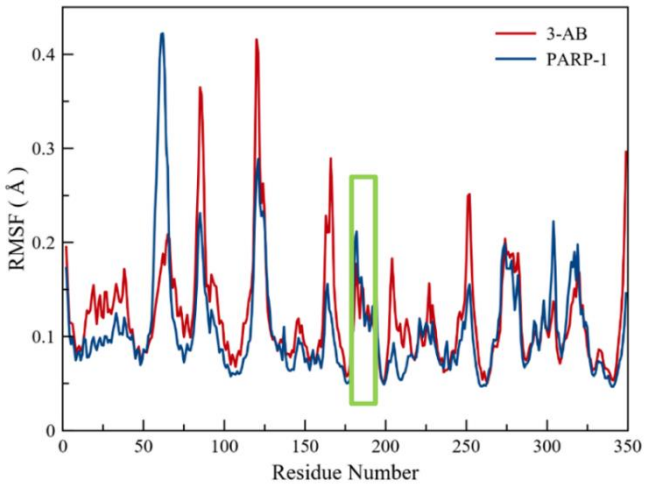


Figure 21. RMSF analysis of PARP-1 and 3-AB (protein-ligand structure) after MD simulations.

On the other hand, when we look at the RMSF results of the SB-7 ligand shown in Figure 22, changes were determined in the residues in the 200-250 range, which is the binding region of the ligand.

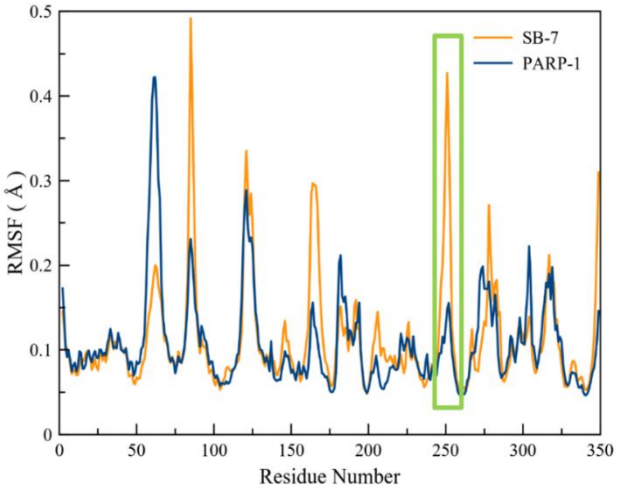


Figure 22. RMSF analysis of PARP-1 and SB-7 (protein-ligand structure) after MD simulations.

4.3. Discussion

Cancer is the most prevalent disease globally, affecting billions of individuals annually. Cancer is a disease characterised by uncontrollable cell proliferation. There are numerous types of cancer, such as breast, lung, and prostate, etc. Prostate cancer is the most frequently diagnosed form of cancer in men. Prostate cancer develops in the prostate gland, which is a part of the male reproductive system. A plethora of therapeutic approaches exist for the treatment of prostate cancer, including surgical, radiotherapy, chemotherapy, and hormone therapy. One of the most significant challenges in the treatment of advanced prostate cancer is the emergence of CRPC. CRPC is an advanced stage of the disease that continues to progress even in the presence of reduced testosterone levels. The development of CRPC involves various mechanisms of resistance, such as activation of AR-independent pathways, intratumoral androgen production, and amplification and mutation of the AR. These resistance mechanisms, including AR amplification and mutation, allow cancer cells to be more sensitive to low androgen levels and remain active despite the low androgen environment . This adaptation enables cancer cells to proliferate and survive despite androgen deprivation therapy (ADT), which contributes to disease advancement. In CRPC, both AR-associated and AR-independent mechanisms are triggered to enhance the proliferation and viability of cancer cells. These insights shed light on the complex nature of CRPC and the underlying mechanisms driving its progression and resistance to treatment. Recently a new approach, PARPi has emerged in the treatment of CRPC. This new treatment strategy represents a significant improvement in the management of this aggressive form of prostate cancer. The PARP-1 controls cellular division and cell death processes, like necrosis, apoptosis, and necroptosis, which affects the cancer cell cycle. Inhibiting the activation of prostate-specific genes like TMPRSS2-ERG and PSMA, which are necessary for AR activation, particularly in CRPC models, is a way that PARP-1 might impact AR signaling. Given that PARP-1 is involved in cancer cells, it is a significant target, particularly when it comes to PARP-1 inhibition in the context of CRPC therapy.

So the thesis aim's was to investigating the effects of novel SB derivatives on the treatment of CRPC by *in vitro* and *in silico* approaches by inhibiting PARP-1 activity.

First of all, cytotoxicities of the compounds were determined on DU145, PC-3 and PNT1-A cells. According to the results, SB-5, SB-7, SB-9 and SB-10 compounds have lower IC_{50} values than 10 uM and SI higher than 2. All of the four compounds have hydoxly group on their R2-R3-R4 functional groups. According to the literature, more OH group can be caused of more cytotoxicity because these groups can disrupt the integrity of cell membranes with their polar and hydrophilic properties, interact with intracellular targets and change the functions of proteins and enzymes. Based on cytotoxicity results, the compounds were selected as lead compounds to determine the anticancer activites. Colony formation, wound healing and qPCR analysis were conducted to determine the anticancer activities of the compounds. According to colony formation assay, SB-7 compound was the most selective to inhibit colony formation capacities of the DU145 cells while on the PC-3 cells, SB-5 and SB-7 compounds were the selective. Correlativly on wound healing assay, IC_{50} application of the SB-5 and SB-7 compounds to inhibit migration capacities of the DU145 cells, more selective and have the best results according to positive control, doxorubicin. Additionally, the affects of migration capabilities on PC-3 cells, SB-7, SB-9 and SB-10 compounds moderately inhibited the migration of cells. While, SB-5 was the most effective compound for the inhibiton of PC-3 cells migration. Based on the these anticancer assays, qPCR analysis was used to determine the types of cell death of the compounds. Bax, BCL-2 and Caspase-3 genes were selected for apoptosis, while LC-3 and Beclin-1 genes were selected for autopaghy detection. Bax is a mammalian protein of the BCL-2 protein family. Increased expression levels of Bax promotes apoptosis. The structural transition of this protein permeabilizes the mitochondrial outer membrane. Instead, Bcl-2 is known as an antiapoptotic protein that blocks apoptosis. The expression levels of Bax increases during apoptosis, while, the expression levels of Bcl-2 decrease (Qian et al., 2022). According to the findings, SB-5, SB-7 and SB-10 compounds increased the relative mRNA expression levels of Bax on DU145 cells but not on PC-3 cells. Therefore, SB-5,SB-7 and SB-10 compounds were increased BCL-2 expression levels on DU145 cells. In order that, Bax/BCL-2 ratios of the compounds were not significant on DU145 cells. Similar to results of DU145 cells, SB-5 and SB-7 compounds increased the BCL-2 expressions lead to low Bax/BCL-2 ratio on PC-3 cells. Instead, SB-10 compound increased BCL-2 expression level which led to supression of Bax/BCL-2 ratio. In order to ascertain whether the compounds induce apoptosis in cells, Caspase-3 expression levels were examined at mRNA levels. Caspase-3 which is normally present as pro-caspase-3. Procaspase-3 is activated in the later

stages of apoptosis and carries out important proteolytic activities that cause cell death. Reviewing the results, none of the compounds had selective significant effects on relative Caspase-3 expression at mRNA levels neither DU145 nor PC-3 cells. Based on the findings, it assumped that the mechanism underlying the cell death may not be related to apoptosis. In order to investigate the sort of cell death, LC-3 and Beclin-1 genes were chosen for autophagy. LC3 is a protein that plays a critical role in the formation and elongation of the autophagosome membrane during the autophagy process and is an important marker of autophagic activity, while Beclin-1 functions as a central component of a protein complex that initiates the onset of the autophagy process and regulates autophagic vesicle formation. Therefore, the expression of these two genes has important activities in the autophagy death pathway. Considering the results on DU145 cells, all of the lead compounds had similar effect on LC3 expression levels. All of them significantly increased the LC3 expressions compared to positive control, doxorubicin. Looking ahead to expression levels of Beclin-1 , all of the compounds increased the expression levels at leat 1.2 fold. Moreover, SB-7 was the most selective that increase Beclin-1 expression, remarkably. However, an analysis of the PC-3 results indicates that the lead compounds appear to suppress LC3 and Beclin-1 expression, rather than induce it.

When we consider the relative mRNA expression level studies conducted in two castration-resistant prostate cancer cells, SB-7 compound stands out in particular. SB-7 compound significantly increased the expression level of genes in LC3 and Beclin genes in DU145 cells. The reason for the difference in cell death patterns in two same cancer-type cell lines may be the characteristic features of the cell lines. When we look at the characteristic features of the cell lines, DU145 cells have a more moderate castration resistance, while the cells metastasize to the brain. On the other hand, PC-3 cells are a highly aggressive cancer cell line and metastasize to the bone. The reason why SB-7 compound selective for DU145 cells may be the PTEN mutation characteristically found in PC-3 cells. Deletion of the PTEN gene is excessively activate the PI3K/Akt/mTOR signaling pathway. Excessive activation of this pathway led have an effect on increasing cell proliferation and survival. The Akt gene, which plays a role in the PI3K/Akt/mTOR signaling pathway, increase cell proliferation by resisting apoptosis. At the same time, the mTOR gene acts as a gene that suppresses autophagy. Its excessive activation in PC-3 cells may suppress cells

from going into autophagy. On the contrary, DU145 cells are a cell line that is more sensitive to inhibition of the mTOR protein. For this reason, the SB-7 compound may have a role in the PI3K/Akt/mTOR signaling pathway. Considering its functions in autophagy, it may inhibit the mTOR gene. More detailed studies are needed to determine this.

After qPCR analysis, *in vitro* PARP-1 inhibition assay was conducted. If we looking ahead the results, SB-5, SB-7, SB-9 and SB-10 compounds were screened at 1-2000 uM doses. According to the IC_{50} values determined after inhbition assay, SB-7 compound has a lower IC_{50} value than the other compounds selected as leads. While the reference compound 3-AB has an IC_{50} value of 2 μM, SB-7 compound has an IC_{50} value of 1.8 mM. If we interpret the results, SB-7 compound does not have a very low IC_{50} value but gives better results than the other selected leads. Based on these findings, compound SB-7 was identified as the most potent precursor compound and further investigations were conducted using MD and molecular docking analyses.

Molecular docking simulations is one of the most frequently used approach, uses in a variety of fields such as drug discovery, structure-activity studies, and virtual screening studies, for understanding and predicting of binding modes of two molecules. Prediction of the best binding mode was determined based on binding affinity. In the current study, firstly, the binding affnities of the SB-7 and reference compound (3-AB) were defined as -9.8 , -5.8 respectively. On the molecular docking analysis, lower binding affinity refers that the ligand binds to the protein more strongely and stable. Looking ahead to interactions, SB-7 compounds had more interactive compared to 3-AB. The SB-7 compound had made more hydrogen bonds than the 3-AB. This is because it has more functional groups that can bond with the protein.

If we look at the protein-ligand MD results after molecular docking, the RMSD values remained below 0.3 nm and no major deviations occurred in the protein-ligand complex. This results suggests that the SB-7 compound maintained a fixed and stable position within the binding site. After protein-ligand MD simulation, binding energies were recalculated. When the results were examined, it was determined that the binding energy for

SB-7 was -11.8 kcal/mol and for 3-AB it was -5.8 kcal/mol. This situation shows that the binding affinity, which was calculated as -9.8 kcal/mol after molecular docking, decreased to -11.8 kcal/mol after MD, indicating that the ligand binds to the protein more stably and strongly. In addition, RMSF analysis was performed and when the results were examined, significant energy changes were determined in the regions where the ligand SB-7 bound to the protein. The reason for this is that the amino acids remained quite flexible in the regions where the SB-7 compound was bound. When the binding energies were examined, these flexible regions had a significant effect on the binding of the ligand to the protein.

CHAPTER 5
CONCLUSION

Upon analyzing the results of all the *in vitro* biological assays, it was observed that compound SB-7 exhibited significant cytotoxicity in both DU145 and PC-3 castration-resistant prostate cancer cell lines. This compound demonstrated a remarkably low IC_{50} value and a high degree of selectivity. Notably, SB-7 exhibited a substantial inhibition of colony formation in the colony formation assay, indicating its potential to impede the proliferation of cancer cells. Furthermore, in the wound healing assay, SB-7 effectively reduced wound healing after a 48-hour time period, surpassing the positive control. In terms of relative mRNA expressions for apoptosis and autophagic cell death types, SB-7 demonstrated a remarkable impact on the expression levels of LC-3 and Beclin-1 in the DU145 cell line, indicating its prominent role in autophagy induction. Additionally, the PARP-1 *in vitro* enzyme inhibition assay revealed that SB-7 outperformed other tested compounds, showcasing its superior efficacy.In addition to biological assays, SB-7 compound has the lowest binding energy compared to reference molecule. Additionally, when the compound binds to the protein, it remains stable at the site and forms a strong bond.

Overall, the results obtained highlight the remarkable cytotoxic potential of SB-7 in castration-resistant prostate cancer cells, along with its ability to modulate key molecular pathways and biomarkers. These findings constitute an important step towards the development of novel therapeutic strategies for CRPC.

REFERENCES

Adcock, S. A., and McCammon, J. A. (2006). "Molecular Dynamics: Survey of Methods for Simulating the Activity of Proteins". *Chemical Reviews*, *106*(5), 1589–1615. https://doi.org/10.1021/cr040426m

Antika, G., Cinar, Z. Ö., Dönmez, S., Seçen, E., Özbil, M., Prandi, C., and Tumer, T. B. (2023). "Effects of Strigolactones on NLRP3 Activation, Nitrosative Stress, and Antioxidant Mox Phenotype: In Vitro and In Silico Evidence". *ACS Bio and Med Chem Au*. https://doi.org/10.1021/acsbiomedchemau.3c00063

Barbieri, C. E., Baca, S. C., Lawrence, M. S., Demichelis, F., Blattner, M., Theurillat, J.-P., White, T. A., Stojanov, P., Van Allen, E., Stransky, N., Nickerson, E., Chae, S.-S., Boysen, G., Auclair, D., Onofrio, R. C., Park, K., Kitabayashi, N., MacDonald, T. Y., Sheikh, K., … Garraway, L. A. (2012)." Exome sequencing identifies recurrent SPOP, FOXA1 and MED12 mutations in prostate cancer". *Nature Genetics*, *44*(6), 685–689. https://doi.org/10.1038/ng.2279

Böttcher, R., Dulla, K., Van Strijp, D., Dits, N., Verhoef, E. I., Baillie, G. S., Van Leenders, G. J. L. H., Houslay, M. D., Jenster, G., and Hoffmann, R. (2016). "Human PDE4D isoform composition is deregulated in primary prostate cancer and indicative for disease progression and development of distant metastases". *Oncotarget*, *7*(43), 70669–70684. https://doi.org/10.18632/ONCOTARGET.12204

Brooks, J. D., Weinstein, M., Lin, X., Sun, Y., Pin, S. S., Bova, G. S., Epstein, J. I., Isaacs, W. B., and Nelson, W. G. (1998). "CG island methylation changes near the GSTP1 gene in prostatic intraepithelial neoplasia". *Cancer Epidemiology, Biomarkers and Prevention : A Publication of the American Association for Cancer Research, Cosponsored by the American Society of Preventive Oncology*, *7*(6), 531–536.

Carlson, H. A., Masukawa, K. M., and McCammon, J. A. (1999). "Method for including the dynamic fluctuations of a protein in computer-aided drug design". *The Journal of Physical Chemistry A*, *103*(49), 10213–10219.

Chen, C. Y., Chen, J., He, L., and Stiles, B. L. (2018). "PTEN: Tumor suppressor and metabolic regulator". *Frontiers in Endocrinology*, *9*(JUL), 1–12. https://doi.org/10.3389/fendo.2018.00338

de Bono, J., Mateo, J., Fizazi, K., Saad, F., Shore, N., Sandhu, S., Chi, K. N., Sartor, O., Agarwal, N., Olmos, D., Thiery-Vuillemin, A., Twardowski, P., Mehra, N., Goessl, C., Kang, J., Burgents, J., Wu, W., Kohlmann, A., Adelman, C. A., and Hussain, M. (2020a). Olaparib for Metastatic Castration-Resistant Prostate Cancer. *New England Journal of Medicine*, *382*(22), 2091–2102. https://doi.org/10.1056/nejmoa1911440

Dönmez, S., Lapinskaite, R., Atalay, H. N., Tokay, E., Kockar, F., Rycek, L., Özbil, M., and Tumer, T. B. (2024). "Selagibenzophenone B and Its Derivatives: SelB-1, a Dual Topoisomerase I/II Inhibitor Identified through In Vitro and In Silico Analyses". *ACS Bio and Med Chem Au*. https://doi.org/10.1021/acsbiomedchemau.4c00027

González-Billalabeitia, E., Seitzer, N., Song, S. J., Song, M. S., Patnaik, A., Liu, X. S., Epping, M. T., Papa, A., Hobbs, R. M., Chen, M., Lunardi, A., Ng, C., Webster, K. A., Signoretti, S., Loda, M., Asara, J. M., Nardella, C., Clohessy, J. G., Cantley, L. C., and Pandolfi, P. P. (2014). "Vulnerabilities of PTEN-TP53-deficient prostate cancers to compound PARP-PI3K inhibition". *Cancer Discovery*, *4*(8), 896–904. https://doi.org/10.1158/2159-8290.CD-13-0230

Gupta, R. A., Shah, N., Wang, K. C., Kim, J., Horlings, H. M., Wong, D. J., Tsai, M. C., Hung, T., Argani, P., Rinn, J. L., Wang, Y., Brzoska, P., Kong, B., Li, R., West, R. B., Van De Vijver, M. J., Sukumar, S., and Chang, H. Y. (2010)." Long non-coding RNA HOTAIR reprograms chromatin state to promote cancer metastasis". *Nature*, *464*(7291), 1071–1076. https://doi.org/10.1038/nature08975

Hussain, M., Mateo, J., Fizazi, K., Saad, F., Shore, N., Sandhu, S., Chi, K. N., Sartor, O., Agarwal, N., Olmos, D., Thiery-Vuillemin, A., Twardowski, P., Roubaud, G., Özgüroğlu, M., Kang, J., Burgents, J., Gresty, C., Corcoran, C., Adelman, C. A., and de Bono, J. (2020). "Survival with Olaparib in Metastatic Castration-Resistant Prostate Cancer". *New England Journal of*

Medicine, *383*(24), 2345–2357. https://doi.org/10.1056/NEJMOA2022485/SUPPL_FILE/NEJMOA2022485_DATA-SHARING.PDF

Kabeya, Y., Mizushima, N., Ueno, T., Yamamoto, A., Kirisako, T., Noda, T., Kominami, E., Ohsumi, Y., and Yoshimori, T. (2000). "LC3, a mammalian homologue of yeast Apg8p, is localized in autophagosome membranes after processing". *EMBO Journal*, *19*(21), 5720–5728. https://doi.org/10.1093/emboj/19.21.5720

Kim, M. J., Cardiff, R. D., Desai, N., Banach-Petrosky, W. A., Parsons, R., Shen, M. M., and Abate-Shen, C. (2002)." Cooperativity of Nkx3.1 and Pten loss of function in a mouse model of prostate carcinogenesis". *Proceedings of the National Academy of Sciences of the United States of America*, *99*(5), 2884–2889. https://doi.org/10.1073/pnas.042688999

Knudsen, E. S., Pruitt, S. C., Hershberger, P. A., Witkiewicz, A. K., and Goodrich, D. W. (2019). "Cell Cycle and Beyond: Exploiting New RB1 Controlled Mechanisms for Cancer Therapy". *Trends in Cancer*, *5*(5), 308–324. https://doi.org/10.1016/j.trecan.2019.03.005

Koivisto, P., Kononen, J., Palmberg, C., Tammela, T., Hyytinen, E., Isola, J., Trapman, J., Cleutjens, K., Noordzij, A., Visakorpi, T., and Kallioniemi, O. P. (1997). "Androgen receptor gene amplification: a possible molecular mechanism for androgen deprivation therapy failure in prostate cancer". *Cancer Research*, *57*(2), 314–319.

Kote-Jarai, Z., Leongamornlert, D., Saunders, E., Tymrakiewicz, M., Castro, E., Mahmud, N., Guy, M., Edwards, S., O'Brien, L., Sawyer, E., Hall, A., Wilkinson, R., Dadaev, T., Goh, C., Easton, D., Goldgar, D., and Eeles, R. (2011). "BRCA2 is a moderate penetrance gene contributing to young-onset prostate cancer: Implications for genetic testing in prostate cancer patients". *British Journal of Cancer*, *105*(8), 1230–1234. https://doi.org/10.1038/bjc.2011.383

Lapinskaite, R., Atalay, H. N., Malatinec, Š., Donmez, S., Cinar, Z. O., Schwarz, P. F., Perhal, A. F., Císařová, I., Labanauskas, L., Karpiński, T. M., Dirsch, V. M., Tumer, T. B., and Rycek, L. (2023). "Synthesis of Selagibenzophenone A and Its Derivatives for Evaluation

of Their Antiproliferative, RORγ Inverse Agonistic, and Antimicrobial Effect**". *ChemistrySelect*, *8*(7). https://doi.org/10.1002/slct.202204816

Le, T. K., Duong, Q. H., Baylot, V., Fargette, C., Baboudjian, M., Colleaux, L., Taïeb, D., and Rocchi, P. (2023). Castration-Resistant Prostate Cancer: From Uncovered Resistance Mechanisms to Current Treatments. *Cancers*, *15*(20), 1–17. https://doi.org/10.3390/cancers15205047

Leongamornlert, D., Mahmud, N., Tymrakiewicz, M., Saunders, E., Dadaev, T., Castro, E., Goh, C., Govindasami, K., Guy, M., O'Brien, L., Sawyer, E., Hall, A., Wilkinson, R., Easton, D., Goldgar, D., Eeles, R., and Kote-Jarai, Z. (2012). "Germline BRCA1 mutations increase prostate cancer risk". *British Journal of Cancer*, *106*(10), 1697–1701. https://doi.org/10.1038/bjc.2012.146

Lian, F., Sharma, N. V., Moran, J. D., and Moreno, C. S. (2015). "The biology of castration-resistant prostate cancer". *Current Problems in Cancer*, *39*(1), 17–28. https://doi.org/10.1016/j.currproblcancer.2014.11.004

Liang, X. H., Kleeman, L. K., Jiang, H. U. I. H. U. I., Gordon, G., Goldman, J. E., Berry, G., Herman, B., Levine, B., Hill, C., and Carolina, N. (1998). *Beclin1-Bcl2*. *72*(11), 8586–8596.

Liu, X., Luo, H. Bin, Huang, Y. Y., Bao, J. M., Tang, G. H., Chen, Y. Y., Wang, J., and Yin, S. (2014). "Selaginpulvilins A-D, new phosphodiesterase-4 inhibitors with an unprecedented skeleton from selaginella pulvinata". *Organic Letters*, *16*(1), 282–285. https://doi.org/10.1021/ol403282f

M.J. Abraham, D. van der Spoel, E. Lindahl, B.Hess, and the G. development team. (2018). *GROMACS User Manual version 2018*.

Mateo, J., Carreira, S., Sandhu, S., Miranda, S., Mossop, H., Perez-Lopez, R., Nava Rodrigues, D., Robinson, D., Omlin, A., Tunariu, N., Boysen, G., Porta, N., Flohr, P., Gillman, A., Figueiredo, I., Paulding, C., Seed, G., Jain, S., Ralph, C., … de Bono, J. S. (2015). "DNA-Repair Defects and Olaparib in Metastatic Prostate Cancer". *New England Journal of*

Medicine, *373*(18), 1697–1708. https://doi.org/10.1056/nejmoa1506859

Mello, S. S., and Attardi, L. D. (2013). "Not all p53 gain-of-function mutants are created equal". In *Cell death and differentiation* (Vol. 20, Issue 7, pp. 855–857). https://doi.org/10.1038/cdd.2013.53

Mendoza, M. C., Er, E. E., and Blenis, J. (2011). "The Ras-ERK and PI3K-mTOR pathways: cross-talk and compensation". *Trends in Biochemical Sciences*, *36*(6), 320–328. https://doi.org/10.1016/j.tibs.2011.03.006

Ozbil, M., Barman, A., Bora, R. P., and Prabhakar, R. (2012). "Computational insights into dynamics of protein aggregation and enzyme–substrate interactions". *The Journal of Physical Chemistry Letters*, *3*(23), 3460–3469.

Qian, S., Wei, Z., Yang, W., Huang, J., Yang, Y., and Wang, J. (2022)." The role of BCL-2 family proteins in regulating apoptosis and cancer therapy". *Frontiers in Oncology*, *12*(October), 1–16. https://doi.org/10.3389/fonc.2022.985363

Rankin, E. B., and Giaccia, A. J. (2016)." Hypoxic control of metastasis". *Science (New York, N.Y.)*, *352*(6282), 175–180. https://doi.org/10.1126/science.aaf4405

Rose, M., Burgess, J. T., O'Byrne, K., Richard, D. J., and Bolderson, E. (2020). "PARP Inhibitors: Clinical Relevance, Mechanisms of Action and Tumor Resistance". *Frontiers in Cell and Developmental Biology*, *8*(September), 1–22. https://doi.org/10.3389/fcell.2020.564601

Scher, H. I., Fizazi, K., Saad, F., Taplin, M.-E., Sternberg, C. N., Miller, K., de Wit, R., Mulders, P., Chi, K. N., Shore, N. D., Armstrong, A. J., Flaig, T. W., Fléchon, A., Mainwaring, P., Fleming, M., Hainsworth, J. D., Hirmand, M., Selby, B., Seely, L., and de Bono, J. S. (2012)." Increased Survival with Enzalutamide in Prostate Cancer after Chemotherapy". *New England Journal of Medicine*, *367*(13), 1187–1197. https://doi.org/10.1056/nejmoa1207506

Schmid, N., Eichenberger, A. P., Choutko, A., Riniker, S., Winger, M., Mark, A. E., and van Gunsteren, W. F. (2011)." Definition and testing of the GROMOS force-field versions 54A7 and 54B7". *European Biophysics Journal*, *40*(7), 843. https://doi.org/10.1007/s00249-011-0700-9

Schreiber, V., Dantzer, F., Amé, J. C., and De Murcia, G. (2006)." Poly(ADP-ribose): Novel functions for an old molecule". *Nature Reviews Molecular Cell Biology*, *7*(7), 517–528. https://doi.org/10.1038/nrm1963

Søndergaard, C. R., Olsson, M. H. M., Rostkowski, M., and Jensen, J. H. (2011). "Improved treatment of ligands and coupling effects in empirical calculation and rationalization of p K a values". *Journal of Chemical Theory and Computation*, *7*(7), 2284–2295.

Tomlins, S. A., Rhodes, D. R., Perner, S., Dhanasekaran, S. M., Mehra, R., Sun, X.-W., Varambally, S., Cao, X., Tchinda, J., Kuefer, R., Lee, C., Montie, J. E., Shah, R. B., Pienta, K. J., Rubin, M. A., and Chinnaiyan, A. M. (2005). "Recurrent fusion of TMPRSS2 and ETS transcription factor genes in prostate cancer". *Science (New York, N.Y.)*, *310*(5748), 644–648. https://doi.org/10.1126/science.1117679

Trott, O., and Olson, A. J. (2010). "AutoDock Vina: improving the speed and accuracy of docking with a new scoring function, efficient optimization, and multithreading". *Journal of Computational Chemistry*, *31*(2), 455–461.

Varambally, S., Dhanasekaran, S. M., Zhou, M., Barrette, T. R., Kumar-Sinha, C., Sanda, M. G., Ghosh, D., Pienta, K. J., Sewalt, R. G. A. B., Otte, A. P., Rubin, M. A., and Chinnaiyan, A. M. (2002). "The polycomb group protein EZH2 is involved in progression of prostate cancer". *Nature*, *419*(6907), 624–629. https://doi.org/10.1038/nature01075

Vivanco, I., and Sawyers, C. L. (2002). "The phosphatidylinositol 3-Kinase AKT pathway in human cancer". *Nature Reviews. Cancer*, *2*(7), 489–501. https://doi.org/10.1038/nrc839

Volinia, S., Calin, G. A., Liu, C. G., Ambs, S., Cimmino, A., Petrocca, F., Visone, R., Iorio, M., Roldo, C., Ferracin, M., Prueitt, R. L., Yanaihara, N., Lanza, G., Scarpa, A., Vecchione, A.,

Negrini, M., Harris, C. C., and Croce, C. M. (2006). "A microRNA expression signature of human solid tumors defines cancer gene targets". *Proceedings of the National Academy of Sciences of the United States of America*, *103*(7), 2257–2261. https://doi.org/10.1073/pnas.0510565103

Yin, D., Li, J., Lei, X., Liu, Y., Yang, Z., and Chen, K. (2014). "Antiviral activity of total flavonoid extracts from selaginella moellendorffii hieron against coxsackie virus B3 in vitro and in vivo". *Evidence-Based Complementary and Alternative Medicine, 2014*. https://doi.org/10.1155/2014/950817

Yin, L., Liu, Y., Peng, Y., Peng, Y., Yu, X., Gao, Y., Yuan, B., Zhu, Q., Cao, T., He, L., Gong, Z., Sun, L., Fan, X., and Li, X. (2018). "PARP inhibitor veliparib and HDAC inhibitor SAHA synergistically co-target the UHRF1/BRCA1 DNA damage repair complex in prostate cancer cells". *Journal of Experimental and Clinical Cancer Research, 37*(1), 1–14. https://doi.org/10.1186/s13046-018-0810-7

Zuhlke, K. A., Robbins, C. M., Tembe, W. D., Wiley, K. E., Isaacs, S. D., Johng, D., Wang, Y., Bizon, C., Yan, G., Gielzak, M., Partin, A. W., Shanmugam, V., Izatt, T., Sinari, S., Craig, D. W., Zheng, S. L., Walsh, P. C., Montie, J. E., Xu, J., … Cooney, K. A. (2012). "*Germline Mutations in HOXB13"*. 141–149.